JOINT EUROPEAN TORUS

JET–P(92)18

F. de Luca, G. Gorini, G.M.D. Hogeweij, A. Jacchia, G. Kramer,
N.J. Lopes Cardozo, P. Mantica, A.C.C Sips
and JET Team

Fourier Analysis of Sawtooth Heat Pulse Propagation and Comparison with Other Methods Using JET Data

Fourier Analysis of Sawtooth Heat Pulse Propagation and Comparison with Other Methods Using JET Data

F. de Luca[1], G. Gorini[1], G.M.D. Hogeweij[2], A. Jacchia[3], G. Kramer,
N.J. Lopes Cardozo[2], P. Mantica[3], A.C.C Sips
and JET Team*

JET-Joint Undertaking, Culham Science Centre, OX14 3DB, Abingdon, UK

[1]Dipartimento di Fisica, Universita degli Studi di Milano, Milano, Italy
[2]FOM Instituut voor Plasmafysica "Rijnhuizen", Associatie EURATOM-FOM, Nieuwegein, The Netherlands
3Instituto di Fisica del Plasma, Associazione EURATOM-ENEA-CNR, Milano, Italy
** See Annex*

Preprint of Paper to be submitted for publication in
Nuclear Fusion

FOURIER ANALYSIS OF SAWTOOTH HEAT PULSE PROPAGATION AND COMPARISON WITH OTHER METHODS USING JET DATA

P.Mantica, F.De Luca*, G.Gorini*, A.Jacchia
Istituto di Fisica del Plasma, Associazione EURATOM-ENEA-CNR, Milano, Italy
**Dipartimento di Fisica, Università degli Studi di Milano, Milano, Italy*

G.M.D.Hogeweij, N.J.Lopes Cardozo
FOM Instituut voor Plasmafysica 'Rijnhuizen', Associatie EURATOM-FOM, Nieuwegein, The Netherlands

G.Kramer, A.C.C.Sips
JET Joint Undertaking, Abingdon, U.K.

ABSTRACT

A new method for the analysis of sawtooth heat pulse propagation is presented. The method is based on Fourier analysis of data where the statistical noise is reduced by a suitable noise reduction procedure. Besides the value of the incremental heat diffusivity (χ^{inc}), information on the magnitude of non-diffusive transport may be extracted, depending on the quality of the data.

The method is illustrated using JET data. A comparison is made with two other methods of analysis of sawtooth heat pulse propagation in use at JET, and good agreement is found among the χ^{inc} values obtained.

1. INTRODUCTION

Understanding the processes that govern transport of particles and energy in a hot, magnetized plasma is today one of the most urgent challenges in magnetic fusion research [1]. With the advent of highly sophisticated diagnostics, measurements of the plasma density and temperature with good spatial and temporal resolution have become available. These allow the study of the transient response of the plasma to perturbations. From such experiments, the *incremental* diffusion coefficients (e.g. $\chi^{inc}=-\partial q/\partial(n\nabla T)$) can

be deduced, which describe the increment of a flux as a reaction to a change of the driving gradient [2,3]. Complementary information can be obtained from an evaluation of the total flux as a function of the driving gradient, which yields the *effective* diffusion coefficients (e.g. $\chi^{eff}=-q/(n\nabla T)$). In a complex thermodynamic system like a magnetized plasma, the incremental and effective diffusion coefficients need not have the same value [4], and this difference can provide information on the underlying transport processes.

The propagation of sawtooth induced heat pulses was the first type of perturbation to be used for tokamak transport studies [5]. Different methods have been developed for the analysis of such perturbations. The simplest approach derives the diffusivity from the time-to-peak of the pulse [6, 7], an extended version of it makes also use of the radial decay of the amplitude [8]. A more general approach, implemented in the ACCEPT code developed at JET [9], solves the linearized transport equations numerically and makes a full fit to the measured traces. The equations are solved either as a Fixed Boundary problem or as an Initial Value problem.

As an alternative to this analysis in the time-domain, Fourier analysis has also been employed [7]. This approach is straightforward for the interpretation of electron temperature modulation experiments [10, 11], but can also be used for the analysis of a sawtooth heat pulse. Using Fourier analysis, the phase velocity and radial amplitude decay of each harmonic component of the signal can be determined. Thus, the (incremental) diffusivity can be found as a function of frequency [12,13].

The simplest approach is to assume that the heat pulse is a purely diffusive process, described by one diffusion coefficient. If other physical effects are present, such as non-diffusive components in the perturbed heat flux [14] or diffusive cross-coupling between temperature and density [15], the analysis may yield a frequency-dependent diffusivity. It turns out that these effects must be relatively strong before a frequency dependence of the diffusivity can be identified given the accuracy of present-day measurements [16]. If such a frequency dependence is not observed, non-diffusive effects may be neglected in the Fourier analysis, and the (frequency averaged) diffusivity can be used as an estimator of the incremental diffusivity.

In practice, the application of Fourier analysis to heat pulse signals is not trivial. In particular, the phase and amplitude information is contained in the first phase of the pulse, whereas the long tail mainly adds noise to the Fourier spectrum (see Fig.2). Straightforward application of Fourier analysis to heat pulse signals generally results in a very poor determination of the phase and

amplitude spectra. This may be partly the reason why this type of analysis has not been pursued extensively. To our knowledge, results of this kind have been published in only one case [7], while problems in the analysis of the slow decay of the sawtooth pulse have been pointed out in Ref.[17].

In this paper we describe a new method for the application of Fourier analysis to sawtooth heat pulses, which allows to reduce the effect of statistical noise on the determination of the diffusivity. We investigate the accuracy of the method in detail, using both a simulation code to generate heat pulse 'measurements' and experimental data from JET. We then compare the results of this new analysis method with two established methods: the extended time-to-peak method and the ACCEPT simulation code. The comparison is done for a set of 20 JET discharges with a variation of plasma conditions. From this comparison, insight is obtained into the various sources of systematic errors that can affect the different analysis methods.

The structure of the paper is as follows. In Sect.2 the theoretical framework for heat pulse propagation analysis from frequency resolved data is outlined [14]. In Sect.3 the new approach for the application of Fourier techniques to sawtooth heat pulses is illustrated with the help of simulated data. An estimate of the statistical uncertainties associated with the noise level typical of JET sawtooth heat pulses is made. In Sect.4 results of the application of the method to JET heat pulses are presented. Finally, in Sect.5 diffusivity values obtained by different methods of analysis applied to a set of JET discharges in different plasma conditions are compared and discussed.

2. MATHEMATICAL DESCRIPTION

The linearised transport equation governing the propagation of a sawtooth electron temperature perturbation $\tilde{T}(t)$ can be written as [14]

$$\frac{3}{2} n_0 \partial_t \tilde{T} - \nabla\left(n_0 \chi \nabla \tilde{T} + n_0 U \tilde{T}\right) = -n_0 \frac{\tilde{T}}{\tau} \qquad (1)$$

Here χ is the incremental diffusivity (henceforth we drop the superscript inc for clarity of notation), n_0 the equilibrium density, $1/\tau$ an effective damping rate and U the incremental heat pinch velocity, which are all functions of the plasma minor radius. It is important to note that, while in the full transport equation the transport coefficients can be a function of n, T, ∇n, ∇T, in this linearised equation χ and U are not functions of the perturbed quantities. In Eq.1, the effect of coupling of the temperature perturbation with other perturbations has been assumed to be negligible. This appears to be a good

approximation in JET: for instance, terms in $\tilde{n}$ and $\nabla\tilde{n}$ can be neglected since, due to the high χ/D values (χ/D~10) [9], the coupling between temperature and density perturbations only affects the tail of the heat pulse.

The equation for the propagation of a single harmonic component T_ω of the temperature perturbation,

$$T_\omega = \frac{1}{\sqrt{2\pi}}\int_{-\infty}^{+\infty}\tilde{T}\,e^{-i\omega t}dt$$

is

$$n_0\left(\frac{3}{2}i\omega+\frac{1}{\tau}\right)T_\omega - \nabla(n_0\chi\nabla T_\omega + n_0 U T_\omega) = 0 \qquad (2)$$

An approximate solution to Eq.2, retaining to lowest order the effects of damping, cylindrical geometry, heat pinch velocity and gradients of n_0 and χ is derived in the Appendix. In terms of the spatial derivatives of the phase (φ) and amplitude (A) of T_ω, which are the experimental observables, this solution is given by

$$-\varphi' \cong \frac{k_0}{\sqrt{2}}\left(1-\frac{\Delta_0}{2}\right) \qquad (3)$$

$$-\left(\frac{A'}{A}+\frac{1}{2r}-\frac{1}{2r_n}+\left(U+\frac{\chi'}{2}\right)\frac{1}{2\chi}\right) \cong \frac{k_0}{\sqrt{2}}\left(1+\frac{\Delta_0}{2}\right) \qquad (4)$$

where $k_0=(3\omega/2\chi)^{1/2}$, $\Delta_0=2/3\omega\tau$, $r_n=-n_0/\nabla n_0$.

The accuracy of these approximate expression has been verified using computer simulations. In Fig.1, the numerical values of $-\varphi'$ and $-A'/A$ from a simulation are compared with the values predicted by Eq.3-4. The simulation is for a cylindrical JET plasma (a=1.3 m) with $U=10r/a$ m/s, $\chi=1+9r^2/a^2$ m^2/s and τ=15 ms for $\omega/2\pi$= 50, 100 and 150 Hz. All quantities are evaluated at r/a=0.5. As one can see, Eq.3-4 are very accurate in this case.

Taking the product of Eq.3 and 4, an expression for χ is obtained,

$$\chi = \frac{\frac{3}{4}\omega}{\varphi'\left[\frac{A'}{A}+\frac{1}{2}\left(\frac{1}{r}-\frac{1}{r_n}\right)+\frac{1}{2\chi}\left(U+\frac{\chi'}{2}\right)\right]} \qquad (5)$$

This expression is derived on more general grounds in Ref.[14] where its accuracy is also discussed. Here we just point out that, while Eq.3-4 are accurate only to lowest order in the parameters Δ_0, $1/k_0(1/r-1/r_n)$, $1/k_0(U+\chi'/2)/2\chi$, Eq.5 is of more general validity [14].

If the convective-like term $U+\chi'/2$ is negligible (i.e. if it is possible to restrict the analysis within the frame of a purely diffusive transport model), the value of χ can be simply determined by

$$\chi_g = \frac{\frac{3}{4}\omega}{\varphi'\left[\frac{A'}{A} + \frac{1}{2}\left(\frac{1}{r} - \frac{1}{r_n}\right)\right]} \qquad (6)$$

Here the subscript g indicates that only geometrical corrections have been retained in the expression for χ (the role of the $1/r_n$ correction is essentially the same as $1/r$, i.e., a known geometrical correction). If a diffusive model does not hold, the presence of a non-negligible heat pinch term or a non-uniform χ profile would then show up in the data analysis as a frequency dependence of $\chi_g(\omega)$, from which the value of the term $U+\chi'/2$ can be estimated (see Ref.[14]). Alternatively, from Eq.3-4 we see that information on the $U+\chi'/2$ term can be derived from a comparison of the values of φ' and A'/A at frequencies high enough that the damping Δ_0 becomes negligible. In both approaches, however, very good accuracy of the measurements is required to provide reliable estimates of the convective term.

3. APPLICATION TO JET SAWTOOTH HEAT PULSES

3.1 Experimental set-up

The JET 12-channel ECE polychromator [18] has been used to measure the evolution of the electron temperature [3]. Its spatial resolution (~ 5 cm) allows the observation of the perturbation of the electron temperature at four to six radial positions, up to 30 cm outside the mixing radius. The sampling rate is usually ~0.5 to 1 ms, which is adequate for resolving the propagation of the heat pulse across the measurement region.

The noise level depends on the toroidal magnetic field and the electrical bandwidth. For typical heat pulse signals (B_T~3 T, 3 kHz electrical bandwidth), the noise equivalent temperature is 15 eV (standard deviation). To improve the signal-to-noise ratio (S/N) of the signals, a coherent addition procedure is applied to a series of identical sawteeth within one discharge. Typically, 10 sawteeth are added, yielding a gain in S/N of a factor 3. Since we treat the sawtooth collapse and the subsequent relaxation as an excursion from the equilibrium profile, a baseline is subtracted from the data, such that only the perturbation is left. Typical data are shown in Fig. 2 (shot 19619), together with the best-fitted ACCEPT simulation.

3.2 Signal processing and error sensitivity

The numerical application of Fourier analysis to the propagation of a heat pulse following a sawtooth collapse requires considerable attention. The straightforward Fourier analysis of a sequence of many sawtooth cycles is not feasible because the period of the sawtooth instability is not constant in time in high T_e plasmas. Moreover, the slow decay of the temperature pulse contains little useful information while its low S/N ratio considerably distorts the Fourier spectrum.

In order to solve these problems, we perform the Fourier integral of one single heat pulse rather than the Fourier series of a periodic signal. This single heat pulse can be obtained by coherent addition of many sawtooth cycles in order to reduce the statistical noise level in the data, as described in sect.3.1 (Fig.2). In this way, the irregularity of the sawtooth period is no longer a problem as long as the time it takes to the heat pulse to reach the plasma boundary is shorter than a sawtooth period, i.e. pulse pile-up effects are negligible. In this limit, we can also arbitrarily prolongue the baseline before and after the heat pulse in order to increase the number of computed points in the spectra, without introducing any spurious features in the data analysis.

Even after coherent addition, however, we find that the residual S/N level in the tail region may still be so high as to require an additional procedure to reduce the contribution of the tail to the spectrum. Of course, one must be very careful on how to choose a data reduction procedure that does not affect those features of the Fourier spectrum one is interested in.

Noise reduction

A noise reduction procedure which stems from the theoretical framework of Sect.2 consists in the multiplication of the data by a damping factor $\exp(-t/\theta)$. This has the effect of giving less weight to the slow distorted part of the heat pulse. Since multiplication by $\exp(-t/\theta)$ is equivalent to a physical damping of the heat pulse (θ has the same role as $2/3\tau$ in Eq.1), it has on φ' and A'/A the effect described by Eq.3-4, and, more important, it does not affect the value of χ determined from Eq.5-6. It must be noted however that, in case the heat pulse is not purely diffusive, the frequency dependence observed in $\chi_g(\omega)$ is reduced by application of the artificial damping. Therefore, in order to preserve the shape of $\chi_g(\omega)$, we must require that the effect of θ be small, i.e., $\Delta_0=\frac{1}{\omega\theta}<<1$. For

the typical JET frequency $\omega/2\pi$=50 Hz this implies $\theta >>$ 3 ms. With this choice of θ values, possible frequency dependencies of χ_g are not masked by the noise reduction procedure.

The Fourier analysis and data reduction procedure can be illustrated using the simulation made for the heat pulse shown in Fig.2. This was obtained with the ACCEPT code, with a uniform χ=5.55 m^2/s, a damping time constant τ=12 ms, no coupling with density and no convective terms. The Fourier analysis of each data channel is performed by computing the power spectrum and the cross-phase and cross-coherency spectra [19] relative to the innermost channel. This is done numerically by adding a number of zero points before and after each data record (typically the total number of points becomes 10 times the original length of the record) after having multiplied by the factor $\exp(-t/\theta)$). A discrete Fourier transform is then performed with standard techniques. The maximum frequency resolution is actually determined by the bandwidth set by the convolution of the true spectrum with the spectrum of the factor $\exp(-t/\theta)$) and can be expressed as $\Delta f \sim 0.25/\theta$. It is then in the order of 10 Hz for a typical value of θ=25 ms. For each frequency, φ' and A'/A are then calculated by best-fitting a straight line to the spatial profile of $\varphi(\omega,r)$ and $\log(A(\omega,r))$. From these values and the known geometrical terms, $\chi_g(\omega)$ is then reconstructed using Eq.6.

The $\chi_g(\omega)$ reconstructed applying this procedure to the simulated case of Fig.2 yields, as expected, the correct value of χ at all frequencies. The sensitivity of the analysis to the presence of statistical noise in the data is studied by superimposing a known random noise level to the simulated data. The random noise is taken to have a Gaussian distribution and we choose a standard deviation σ=7 eV which is consistent with the noise level observed in the data of Fig.2. This corresponds to a noise level of ~6% in the outermost channel.

Error evaluation

The standard deviation for the determination of χ_g at each frequency is determined by the distribution of χ_g values from a large number of cases where the simulated data have been perturbed with the same level of random noise. The result obtained without using the artificial damping procedure is shown in Fig.3a, where the $\chi_g(\omega)$ obtained in one case and the associated standard deviation $\sigma(\omega)$ are shown. Due to noise, the data loose their cross-

coherency above a certain frequency or, viewed in another way, $\sigma(\omega)$ is very large at high frequencies.

The reduction of the effect of noise obtained by applying a damping factor θ=25 ms to the same data is illustrated in Fig.3b. As one can see, the uncertainty on $\chi_g(\omega)$ is significantly reduced and the useful frequency range is extended. Typically, at these noise levels a maximum frequency of 80-90 Hz is attainable for χ~6 m^2/s, with an uncertainty on χ_g at each frequency ranging from 20% to 30%. For lower values of χ, the relative error is similar, but the frequency range available is reduced (maximum frequency of 50Hz for χ~2 m^2/s). The standard deviation as a function of frequency can be determined with the same procedure also for the quantities φ' and A'/A and is shown in Fig.4 for the same case of Fig.3b. Typical values for the relative uncertainty around 60 Hz are ~20% for φ' and 10% for A'/A.

It is interesting to note that statistical uncertainties are the main limiting factor in the observation of a frequency dependence of χ_g (see also [14]). On the other hand, if no frequency dependence is observed on χ_g, a weighted average of the χ_g values at different frequencies can be performed. This average ($\chi^{FOURIER}$) is obviously a more accurate determination of χ. Due to the correlation among data points introduced by the finite bandwidth (~10 Hz), the uncertainty on $\chi^{FOURIER}$ is larger than would be expected if the data were independent. It is typically ±15% for the heat pulses analyzed in this work.

Apart from this statistical uncertainty, systematic errors due to the relative calibration of the ECE polychromator channels or to the determination of the measurement positions may be present. They would affect the absolute value of χ determined, but have a negligible effect on the frequency dependence of $\chi_g(\omega)$. These kind of uncertainties cannot be investigated by comparison with different methods of analysis, since they affect all methods in the same way.

4. RESULTS

In this section, we illustrate in detail the results of the application of the above described method to the JET sawtooth heat pulse 19619 (Fig.2). This is a 3 MA, 3T limiter bounded discharge with additional heating power (ICRH) P_{add}=5.7 MW. Three channels are available for heat pulse propagation analysis in the region r/a=0.57-0.71. The sampling time was Δt=0.7 ms for a duration of 125 ms (a total of 180 points).

Figs.5a,b show the cross-phase and amplitude spectra of the intermediate channel without and with use of the damping factor θ. One can clearly see

that the use of the artificial damping is essential to eliminate the large oscillations due to the effect of statistical noise. A θ=25 ms value is found to be appropriate, since lowering it further does not improve the results. For the case with the application of the damping factor, Fig.6a,b show amplitudes and phases as a function of radius for different frequencies, from which $\varphi'(\omega)$, $A'/A(\omega)$ and $\chi_g(\omega)$ are determined. The $\chi_g(\omega)$ values are calculated every 10 Hz (approximately corresponding to the bandwidth) and are shown in Fig.7. The values obtained without the use of the damping factor are also plotted to show that the scatter of the χ_g values is greatly reduced by the application of this technique. If the separate values of φ' and A'/A are needed, the values obtained from the line fit of Fig.6 must be corrected for the effect of the artificial damping θ, using Eq.3-4 (or Eq.A3-A4 for large Δ values) to provide the true values of φ', A'/A . These are plotted as functions of frequency in Fig.8.

We first note from Fig.7 that no frequency dependence is observed outside the statistical uncertainties. These would allow values of the term $(U+\chi'/2)/2\chi$ ranging from -14 to 0.5 m^{-1}. On the other hand, comparison of the values of φ' and A'/A above 60 Hz, where the effect of the physical damping (τ) can be considered negligible, yields $(U+\chi'/2)/2\chi < 1.3\pm1.3$ m^{-1}. Therefore, only small values of the convective term are consistent with the data, and the heat pulse can be regarded as purely diffusive. The error on χ due to the neglect of the term $U+\chi'/2$ in Eq.6 is less than 10% in this case. In general, as has been shown in [14], very large values of the parameter $(U+\chi'/2)$ are necessary to give a significant error on χ. The absence of a frequency dependence also confirms a posteriori the validity of the assumption made in Sect.2 that the effect of coupling on the determination of χ is negligible. A weighted average of $\chi_g(\omega)$ over the available frequency range (i.e., $20<\omega/2\pi<80$ Hz in this case) can then be performed to improve further the statistical accuracy of the χ estimate. This yields $\chi^{FOURIER}$ =6.1 m^2/s with a statistical uncertainty of ±15%. This is the typical statistical uncertainty of the incremental χ that can be obtained by Fourier analysis. The investigation of non-diffusive effects, which is the new potentiality of the method, can be quantitatively improved only if data of better quality become available.

5. COMPARISON WITH OTHER METHODS

In this section we compare three different analysis techniques to extract an experimental estimate of the incremental diffusivity χ from the analysis of sawtooth induced heat pulse propagation. Besides the Fourier method

described above, we use the extended time-to-peak method [8] and the numerical modelling and fitting with the ACCEPT code [9]. The three techniques are summarized in Table 1. They provide three experimental estimators of χ which we will call χ^{TTP}, $\chi^{FOURIER}$ and χ^{ACCEPT}. We want to investigate the possible bias of these estimators.

There are various known sources of systematic errors besides the calibration problems mentioned in sect.3.2: for instance, strong cylindrical geometry corrections near the centre, boundary effects near the edge, non-circular geometry of the flux surfaces, strong radial variation of χ (as due for example to a very low χ value inside the mixing radius), presence of a heat pinch, coupling to density pulse (and possibly ion temperature pulse, or momentum pulse), etc. These sources of systematic error may affect the three different analysis methods in different ways, since the methods are sensitive to different aspects of the signals.

The TTP-method only uses the position and height of the peak of the heat pulse: it is insensitive to the behaviour of the signal in the tail of the pulse, and the result is dominated by low Fourier components in the signal. It is insensitive to damping and in the standard formulation it assumes cylindrical geometry. It does not take into account coupling, convection and non-uniform profiles.

The ACCEPT code fits a numerical solution of the transport equations to the signals at different radial positions. The sensitivity of this fit is strongly biased to the lowest frequencies, since, unlike in the case of the TTP-method, the entire signal contributes to the result. In the ACCEPT code, the equations are solved in the actual geometry, including elongation and triangularity. The code can take into account possible convection and damping, and the effect of radial profiles of χ and density. If measurements of the density pulse are available, also the coupling between the temperature and density pulses can be taken into account.

The $\chi^{FOURIER}$ obtained by a weighted average of χ_g values from Fourier analysis over a frequency range is biased to higher frequencies in the signal than χ^{ACCEPT} and χ^{TTP}. Also the Fourier method is insensitive to damping and assumes cylindrical geometry. The effect of convection and χ profile on the χ estimate is small unless very high values of U/χ and χ'/χ are present. A method to account for coupling using the Fourier method is published in [15].

In conclusion, the methods have a number of essential differences, and by comparing the different methods, insight into the various sources of systematic error may be obtained.

First, a straight-forward comparison of the methods is obtained by applying the TTP-method and the Fourier-method to simulated signals produced with the ACCEPT code. If the simulations are done for a purely diffusive system, in cylindrical geometry, with uniform n_e and χ, we find $\chi^{FOURIER} = \chi^{TTP} = \chi^{ACCEPT}$ to a very good accuracy, as expected. This exercise shows that there are no trivial errors in the methods.

Second: the expressions for $\chi^{FOURIER}$ and χ^{TTP} have been derived for a region where cylindrical geometry effects are small. It has been shown in [14] that for $kr<2$ or $k(a-r)<2.5$ (with $k=(3\omega/2\chi)^{1/2}$ as in Sect.2) the error on $\chi^{FOURIER}$ can exceed 10%. For JET, an overestimate of χ larger than 10% is foreseen in a measurement region with r/a>0.8. Besides this, in a D-shaped plasma, with radially varying elongation, cylindrization of the problem may lead to systematic errors. These stem from the mapping of the flux-coordinates (in which system the transport process is defined) onto the radial coordinates (in which system the transport equations are solved). In JET, the correction due to the use of the measurement region geometry rather than the last flux surface geometry is usually fairly small, <20%. If the geometry of the flux surfaces is known (e.g. from an equilibrium code), the correction can be computed independently of the heat pulse measurements. All values of $\chi^{FOURIER}$ and χ^{TTP} reported in this paper have been corrected in this way.

Third: a non-uniform χ can affect χ^{TTP} if the scale length of χ is not large compared to the scale length of the temperature perturbation. In [8] it was shown that χ^{TTP} could show a systematic error of order 10% if χ varied by a factor of 10 over the minor radius. Simulations of JET heat pulse data using the ACCEPT code have shown that even larger ranges may occur. In low-q_a discharges, χ was found to vary from ~0.3 m^2/s in the sawtooth inversion region to ~10 m^2/s at the edge. This leads to a systematic underestimate of χ up to 30%. $\chi^{FOURIER}$ is insensitive to the presence of a low χ inside the mixing radius, while the effect of χ' in the measurement region can be estimated from Eq.5 and is generally small (e.g. take $\chi=1+9r^2/a^2$ m^2/s, then at $r/a=0.6$ $\chi'/4\chi \sim 0.5$ m^{-1}, to be compared with $A'/A \sim 7.5$ m^{-1} at 50 Hz for $\chi=6$ m^2/s. In this case, neglecting the χ' term would introduce a systematic underestimate of χ of ~7%). With the ACCEPT code it is possible to give a χ-profile, because here the evolution of the T_e-profile in the entire plasma cross-section is simulated.

Fourth: coupling between the heat and density pulses can affect the analysis in two distinct ways. Firstly, it implies that the propagation of the heat pulse is governed by the eigenvalue of the 2x2 linearized transport matrix. In the general case, this eigenvalue is not identical to the incremental χ.

Secondly, the shape of the heat pulse is affected by the contribution from the density pulse. As a result, the pulse shape is different from what is expected in the case of pure, uncoupled diffusion. This may lead to non-trivial systematic errors when determining the position of the peak in the signal or when fitting a simulated (uncoupled) heat pulse to the data, and introduces frequency dependent features in the Fourier analysis. Coupling can be treated by the ACCEPT and FOURIER methods only if the density pulse is measured simultaneously with the heat pulse. In JET, the effect of coupling has been evaluated for a series of pulses [9,20]. It was shown that if coupling was not taken into account in the analysis, χ^{ACCEPT} gives an overestimate of χ by <20%. An important finding is that for the interpretation of the density pulse it is essential to take coupling into account [21].

In order to evaluate the cumulative effect of systematic errors on the evaluation of χ, we applied all three methods to heat pulse data from 20 different JET discharges. These include three different plasma currents: I_p=2 MA, 3 MA, 5 MA. As a consequence, the measurement region was located at different positions: r/a=0.5, 0.65, 0.8. Within each group with the same plasma current, the discharge conditions differ in parameters like density, total input power, Z_{eff}. Thus, a large range of χ values is obtained. The results are presented in Fig.9 and Table 2. For this comparison, possible coupling with the density pulse is not taken into consideration by any of the methods.

The general conclusion is that the results of the three methods are strongly correlated. Considering all three groups of data together, it is found that the methods have systematic differences of <30% (see Fig.9 and Table 2). The statistical error of the ratios χ^{TTP}/χ^{ACCEPT} and $\chi^{FOURIER}/\chi^{ACCEPT}$ is ~±15% (see Table 2). The ACCEPT and Fourier methods generally agree well. The overestimate of $\chi^{FOURIER}$ observed in the 5 MA discharges is attributed to the very external position of the measurement region. The TTP-method systematically comes out lower than the other methods. One reason is that the standard formula used to calculate χ^{TTP} (χ^{TTP}=4.3 $a\, v^{HP}/\alpha$, with a the cylindrized minor radius, v^{HP} the heat pulse velocity, α the radial damping rate) was derived in the original paper [8] for measurements taken around $r=r_{mix}+0.15a$, where r_{mix} is the mixing radius. For the 2 MA group of discharges, the measurements were taken at $r=r_{mix}+0.1a$, and this is shown in [8] to yield an underestimate of χ of about 15%. It should be noticed that it is possible to correct for this systematic error by using the complete formula given in [8]. A second reason is the effect of non-uniform χ discussed above, which is strongest in the 5 MA (low q_a) group of discharges.

The substantial agreement among the three methods is in contrast with the TFTR results reported in [22], where a ballistic model is invoked to explain the discrepancies among χ values obtained with different methods. The results described above do not provide any evidence for 'ballistic' heat pulse propagation.

Finally, we remark that for a refined analysis different methods should be applied to the same data, in order to detect systematic errors in the determination of χ. Otherwise, depending on the application, one or another technique can be chosen, according to the following considerations.

The TTP-method is the simplest to apply and most transparent. This makes it very useful for rapid analysis of large data sets and determination of scaling laws, as done in [23]. However, the correct determination of the position of the peak may become hard in the presence of a high S/N ratio. Also, the fact that it is based on an Initial Value problem makes it more subject to systematic errors.

The ACCEPT-method is the most complete one. It can take into account many different effects provided the quality of the data allows the identification of a large number of free parameters. Obviously, it is the most complex to use and may give rise to ambiguity of interpretation. Because of the large amount of computer time required it is more suitable for detailed analysis of selected data sets.

The Fourier method may not be very transparent, since all the analysis is shifted from the time to the frequency domain. However, it provides an alternative insight into the data and can provide direct evidence on the role on non-diffusive terms. It is sensitive to the presence of statistical noise, especially at high frequency. The method is fast and fully automated so it can be used for routine data analysis.

6. CONCLUSIONS

A new method for the determination of the incremental heat diffusivity (χ^{inc}) from analysis of sawtooth heat pulse propagation has been presented. The method is based on Fourier analysis and provides an alternative insight into the heat pulse propagation problem, allowing the investigation of frequency dependent features such as due to non-diffusive transport. This new potentiality of the method relies critically on the availability of data with very good S/N ratio.

The value of χ^{inc} determined by the Fourier method has been compared with those obtained with the time-to-peak method and ACCEPT code using a representative set of JET discharges. The comparison shows that systematic discrepancies among the methods do not exceed 30%, while the statistical uncertainty is around ±15%. The Fourier and ACCEPT methods agree well, while the time-to-peak method has a tendency to underestimate χ by ~ 20%. This level of accuracy is adequate for the determination of scaling laws for χ^{inc} on the basis of perturbative experiments.

ACKNOWLEDGMENTS

We are indebted to the JET electron temperature group for making the ECE polychromator data available.

APPENDIX: APPROXIMATE EXPRESSIONS FOR ϕ' AND A'/A

Starting from Eq.2, we determine analytical expressions for φ' and A'/A which can be developed to lowest order to provide Eq.3-4. The approach is the same as in Ref.[14]. We write T_ω in the form

$$T_\omega = \exp(-\kappa(x)x) \qquad \text{(A1)}$$

where $x=r-r_0$ is a new coordinate system relative to the radius r_0, where φ' and A'/A are to be evaluated. Substituting Eq.A1 into Eq.2, we obtain

$$(\kappa + \kappa' x)^2 - \left(\frac{1}{x_0 + x} - \frac{1}{r_n} + \frac{\chi'}{\chi} + \frac{U}{\chi}\right)(\kappa + \kappa' x) -$$

$$- \left[k^2_{\perp} + \frac{1}{\tau\chi} - \frac{U}{\chi}\left(\frac{1}{x_0 + x} - \frac{1}{r_n}\right) - \frac{U'}{\chi}\right] - (\kappa + \kappa' x)' = 0 \qquad \text{(A2)}$$

This can be solved as an algebraic equation in $\kappa+\kappa' x$. Since

$$\kappa + \kappa' x = -\frac{A'}{A} - i\varphi',$$

the real and imaginary part of the solution provide an analytical expression for φ' and A'/A, respectively.

Choosing the outward propagating root, we find:

$$-\varphi' = \frac{k}{\sqrt{2}}\left[\left(1+\Delta^2\right)^{\frac{1}{2}} - \Delta\right]^{\frac{1}{2}} \tag{A3}$$

$$-\left[\frac{A'}{A} + \left(\frac{1}{2r} - \frac{1}{2r_n}\right) + \left(U + \frac{\chi'}{2}\right)\frac{1}{2\chi}\right] = \frac{k}{\sqrt{2}}\left[\left(1+\Delta^2\right)^{\frac{1}{2}} + \Delta\right]^{\frac{1}{2}} \tag{A4}$$

where

$$k^2 \equiv \frac{3\omega}{2\chi} - \varphi''$$

$$\Delta \equiv \frac{D}{k^2} \equiv \frac{2}{3\omega\tau} + \frac{1}{k^2}\left[-\frac{U}{\chi}\left(\frac{1}{r} - \frac{1}{r_n}\right) - \frac{U'}{\chi} + \left(\frac{1}{2r} - \frac{1}{2r_n} + \frac{U+\chi'}{2\chi}\right)^2 - \left(\frac{A'}{A}\right)'\right]$$

Clearly, these expressions are of little use unless φ'' and $(A'/A)'$ are known, at least approximately.

Expressions for φ'' and $(A'/A)'$ can be obtained by taking the derivative of $\kappa+\kappa' x$ as determined from Eq.A2. The result is

$$\varphi'' = \frac{1}{2k\sqrt{2}} \frac{1}{\left(1+\Delta^2\right)^{\frac{1}{2}}} \left\{\left(k_0^2 \frac{\chi'}{\chi} + \varphi'''\right)\left[\left(1+\Delta^2\right)^{\frac{1}{2}} + \Delta\right]^{\frac{1}{2}} + D'\left[\left(1+\Delta^2\right)^{\frac{1}{2}} - \Delta\right]^{\frac{1}{2}}\right\} \tag{A5}$$

$$\left(\frac{A'}{A}\right)' = \frac{1}{2k\sqrt{2}} \frac{1}{\left(1+\Delta^2\right)^{\frac{1}{2}}} \left\{\left(k_0^2 \frac{\chi'}{\chi} + \varphi'''\right)\left[\left(1+\Delta^2\right)^{\frac{1}{2}} - \Delta\right]^{\frac{1}{2}} - D'\left[\left(1+\Delta^2\right)^{\frac{1}{2}} + \Delta\right]^{\frac{1}{2}}\right\} \tag{A6}$$

In order to develop the above expressions, we assume that the quantities involved satisfy the following ordering:

$\Delta_0 << 1$ (small expansion parameter);

$$\frac{1}{k_0}\left(\frac{1}{r} - \frac{1}{r_n}\right) \sim \frac{1}{k_0}\frac{U}{\chi} \sim \frac{1}{k_0}\frac{\chi'}{2\chi} \sim \Delta_0$$

$$\frac{1}{{k_0}^2}\frac{U'}{\chi} \sim \frac{\varphi'''}{k_0^3} \sim \frac{D'}{k_0^3} \sim {\Delta_0}^2$$

Then, to lowest order in Δ_0,

$$\Delta \cong \Delta_0 - \frac{1}{k_0\sqrt{2}}\frac{\chi'}{2\chi}$$

$$k^2 \cong k_0^2\left(1 - \frac{1}{k_0\sqrt{2}}\frac{\chi'}{2\chi}\right)$$

When these two expressions are substituted into Eq.A3-A4, Eq.3-4 are obtained.

References

[1] Callen, J.D., Phys. Fluids B **8** (1990) 2869, and following Transport Task Force papers.

[2] Lopes Cardozo, N.J., Plasma Phys. and Controlled Fusion **32** (1990) 983.

[3] Tubbing, B.J.D., Lopes Cardozo, N.J., Van der Wiel, M.J., Nucl. Fusion **27** (1987) 1843.

[4] Gentle, K.W., Phys. Fluids **31** (1988) 1105.

[5] Callen, J.D., Jahns, G.L., Phys. Rev. Lett. **38** (1977) 491.

[6] Soler, M., Callen, J.D., Nucl. Fusion **19** (1979) 703.

[7] Fredrickson, E.D., Callen, J.D., McGuire, K., et al., Nucl. Fusion **26** (1986) 849.

[8] Lopes Cardozo, N.J., Tubbing, B.J.D., Tibone, F., Taroni, A., Nucl.Fusion **28** (1988) 1173.

[9] Hogeweij, G.M.D., O'Rourke, J., Sips, A.C.C., Plasma Phys. and Controlled Fusion **33** (1991) 189.

[10] Jahns, G.L., Wong, S.K., Prater, R., Lin, S.H., Ejima, S., Nucl. Fusion **26** (1986) 226.

[11] Ashraf, M., Bishop, C.M., Connor, J.W., et al., in Plasma Physics and Controlled Nuclear Fusion Research 1988 (Proc. 12th Int. Conf. Nice, 1988), Vol.1, IAEA, Vienna (1989) 275.

[12] Bruschi, A., De Luca, F., Gorini, G., Jacchia, A., Lopes Cardozo, N.J., Mantica, P., in Controlled Fusion and Plasma Heating (Proc. 17th Eur. Conf. Amsterdam, 1990), Vol.14B, Part I, European Physical Society (1990) 170.

[13] De Luca, F., Gorini, G., Jacchia, A., Mantica, P., Hogeweij, G.M.D., Lopes Cardozo, N.J., in Controlled Fusion and Plasma Physics (Proc. 18th Eur. Conf. Berlin, 1991), Vol.15C, Part I, European Physical Society (1991) 277.

[14] Jacchia, A., Mantica,P., De Luca, F., Gorini, G., Phys.Fluids B **3** (1991) 3033.

[15] Hogeweij, G.M.D., Lopes Cardozo, N.J., De Luca, F., Gorini, G., Jacchia, A., Mantica, P., The analysis of coupled heat and particle transport in tokamaks by means of Fourier transforms, to be published in Plasma Phys. and Controlled Fusion.

[16] De Luca, F., Gorini, G., Hogeweij, G.M.D., Jacchia, A., Lopes Cardozo, N.J., Mantica, P., in Diagnostics for Contemporary Fusion Experiments

(Proc. Course and Workshop Varenna, 1991), Vol.x, Societa' Italiana di Fisica, Bologna (1992) xxx.

[17] Riedel, K.S., Eberhagen, A., Gruber, O., et al., Nucl.Fusion **28** (1988) 1509.

[18] Sillen, R.M.J., Piekaar, H.W., Werner, W., Infrared Phys. **24** (1984) 511.

[19] Bendat, J.S, Piersol, A.G, Random data: analysis and measurement procedures, Wiley-Interscience, USA (1971).

[20] de Haas, J.C.M, O'Rourke, J., Sips, A.C.C, Lopes Cardozo, N.J., Nucl.Fusion **31** (1991) 1261.

[21] Sips, A.C.C, Hogeweij, G.M.D., Costley, A.E., O'Rourke, J., Lopes Cardozo, N.J., de Haas, J.C.M, Nucl.Fusion **31** (1991) 1545.

[22] Fredrickson, E.D., McGuire, K., Cavallo, A., et al., Phys. Rev. Lett. **65** (1990) 2869.

[23] Lopes Cardozo, N.J. and de Haas, J.C.M, Nucl.Fusion **30** (1990) 521.

TABLE 1
Characterization of three different methods to obtain an estimator for χ from sawtooth heat pulse propagation measurements.

method	estimator	characterization of the method
extended time-to-peak	χ^{TTP}	Uses time-to-peak and amplitude decay. Is based on Initial Value problem. Is insensitive to damping. Geometry: cylindrical
numerical modelling and fitting with the ACCEPT code	χ^{ACCEPT}	The code fits simulated traces to the measurements. Can solve the transport equations either as Initial Value or Forced Boundary problem. Includes conduction, convection, damping and coupling of heat and particle transport. Geometry: Lao-Hirshman representation.
Fourier method	$\chi^{FOURIER}$	Yields χ as a function of the harmonic frequency in the signal. Can provide a diagnostic on the importance of non-diffusive transport. Is insensitive to damping. Geometry: cylindrical.

TABLE 2

Comparison of χ estimates obtained by applying three different methods to a set of 20 JET discharges. The numbers between the groups are group-averages and corresponding percentage deviations. The final numbers refer to the whole data-set.

SHOT	I_p (MA)	χ^{TTP}	χ^{ACCEPT} (m^2/s)	$\chi^{FOURIER}$	χ^{TTP}/χ^{ACCEPT}	$\chi^{FOURIER}/\chi^{ACCEPT}$
15011	2	2.0	2.7	2.6	0.74	0.96
15015		1.1	1.5	1.8	0.73	1.20
15016		1.5	2.2	2.3	0.68	1.05
15017		1.7	2.3	2.3	0.74	1.00
15018		1.3	2.2	2.2	0.59	1.00
15020		1.5	2.4	3.1	0.62	1.29
					0.68±10%	1.08±12%
19356	3	5.4	6.3	5.9	0.86	0.94
19596		3.2	4.2	3.2	0.76	0.76
19611		3.2	3.0	3.8	1.07	1.27
19614		5.0	6.6	5.4	0.76	0.82
19619		5.5	5.6	6.1	0.98	1.09
					0.89±16%	0.98±21%
10907	5	4.4	5.6	8.1	0.79	1.45
10942		3.7	5.0	7.6	0.74	1.52
10944		5.0	6.3	6.7	0.79	1.06
10976		6.5	6.9	8.6	0.94	1.25
10979		4.4	6.2	8.6	0.71	1.39
10980		6.2	7.5	9.5	0.83	1.27
10994		4.7	6.2	6.7	0.76	1.08
10999		4.8	5.9	5.3	0.81	0.90
11008		3.2	5.4	6.7	0.59	1.24
					0.77±12%	1.24±16%
				TOTAL	0.77±15%	1.13±18%

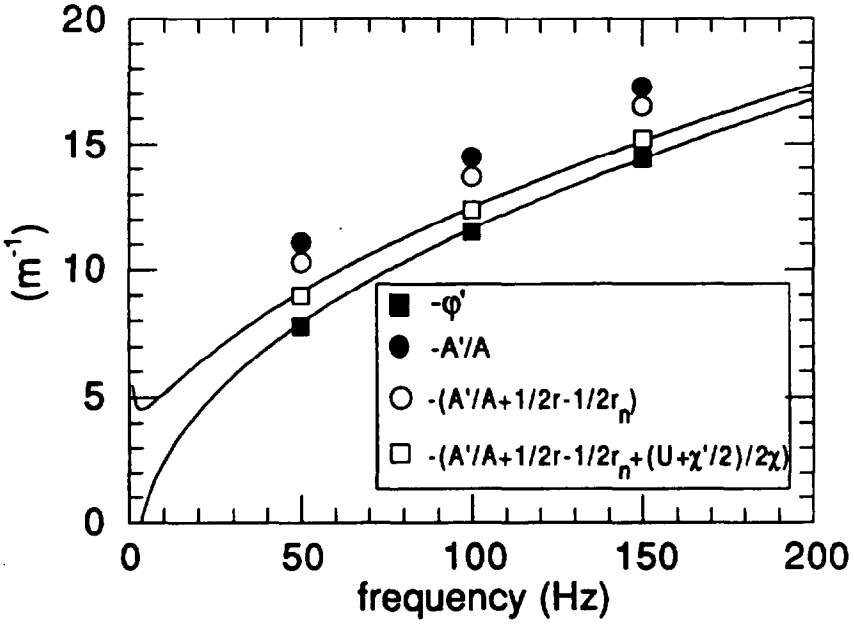

Fig.1: Numerically simulated values of $-\varphi'$ and $-A'/A$ (symbols) compared with the values predicted by Eq.3-4 (full lines). The simulated heat pulse is taken at r/a=0.5 in a cylindrical JET-like plasma (a=1.3 m) with U=10r/a m/s, χ=1+9r^2/a^2 m^2/s and τ=15 ms.

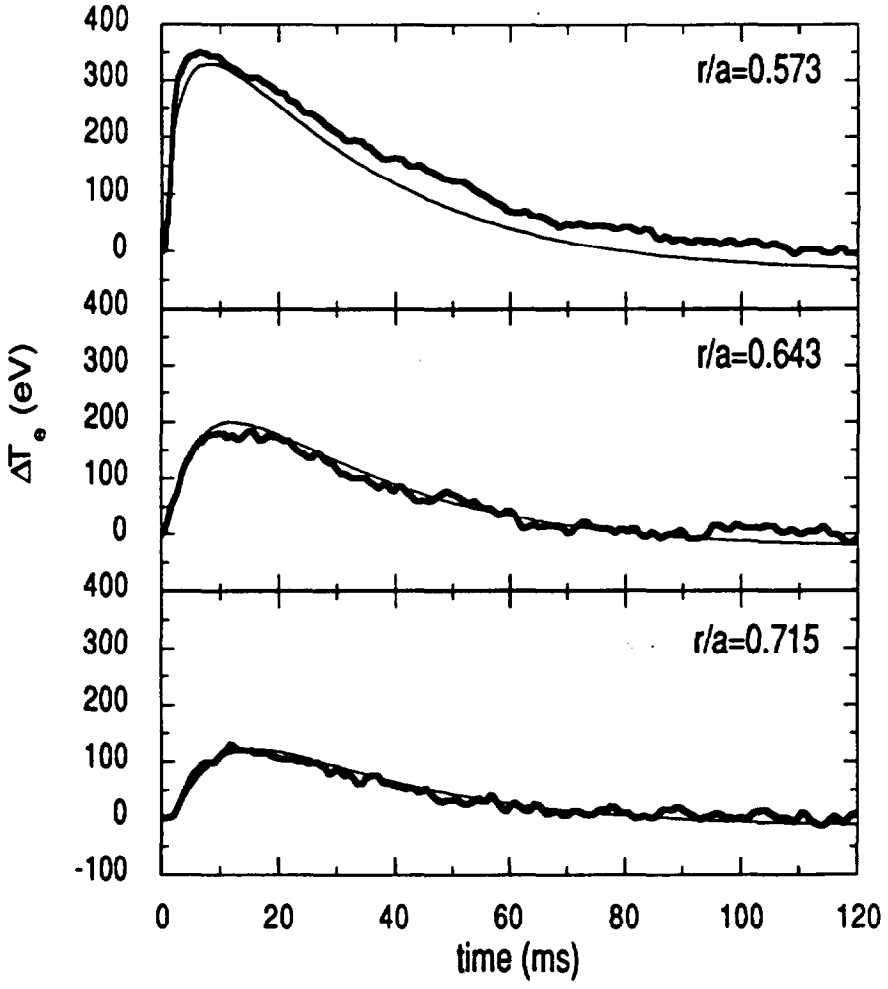

Fig.2: Average heat pulse signals obtained by coherent addition of sawtooth heat pulses for JET discharge #19619. The data (thick line) correspond to the three radial positions r/a=0.573, 0.643 and 0.715. Also shown is the best-fitted ACCEPT simulation (thin line), using a uniform χ=5.55 m^2/s and a damping time constant τ=12 ms.

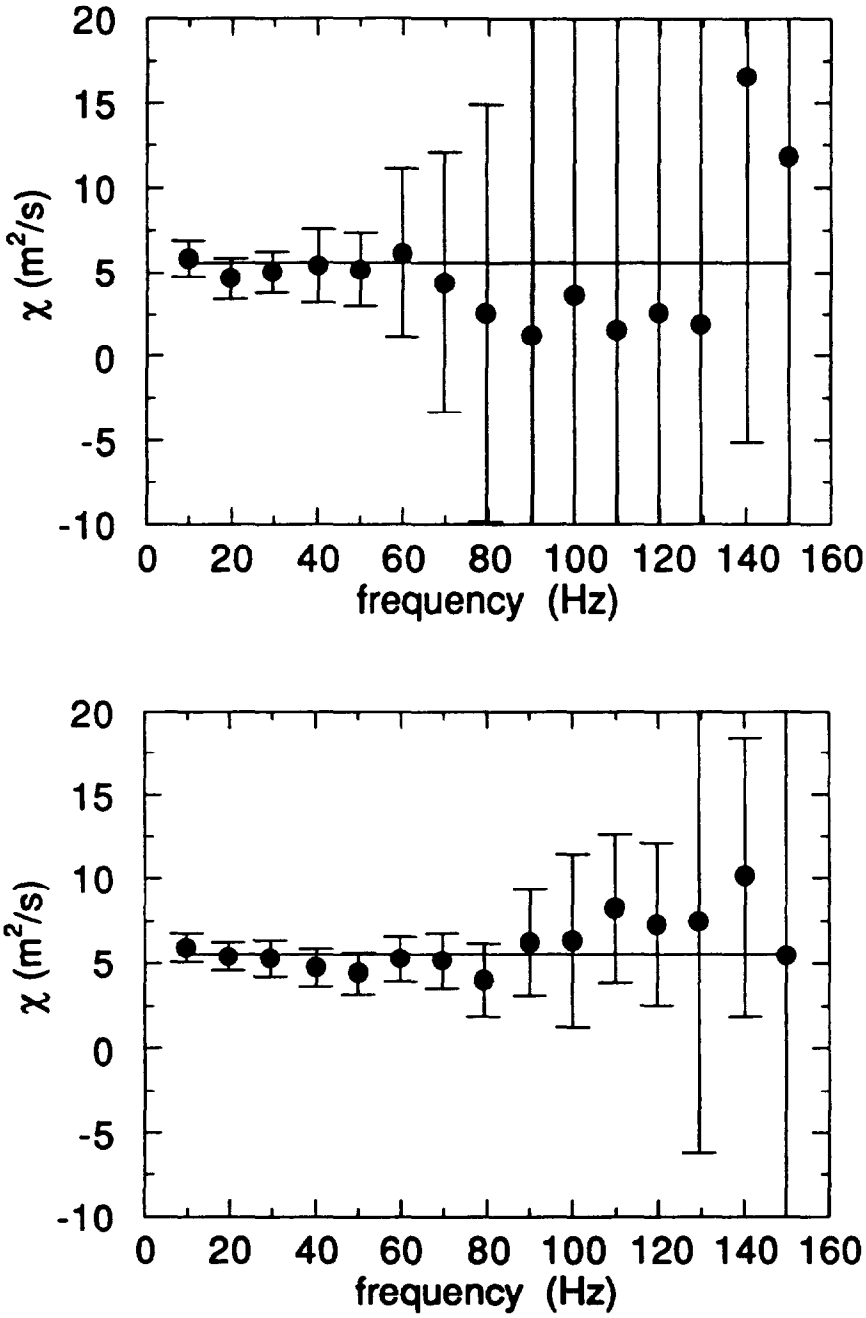

Fig.3: Statistical uncertainties on $\chi_g(\omega)$ obtained by superimposing random noise (σ=7 eV) to the ACCEPT simulation shown in Fig.2, (a) without and (b) with noise reduction using an artificial damping θ=25 ms. The line corresponds to the unperturbed result, the points to one of the many different perturbed cases considered.

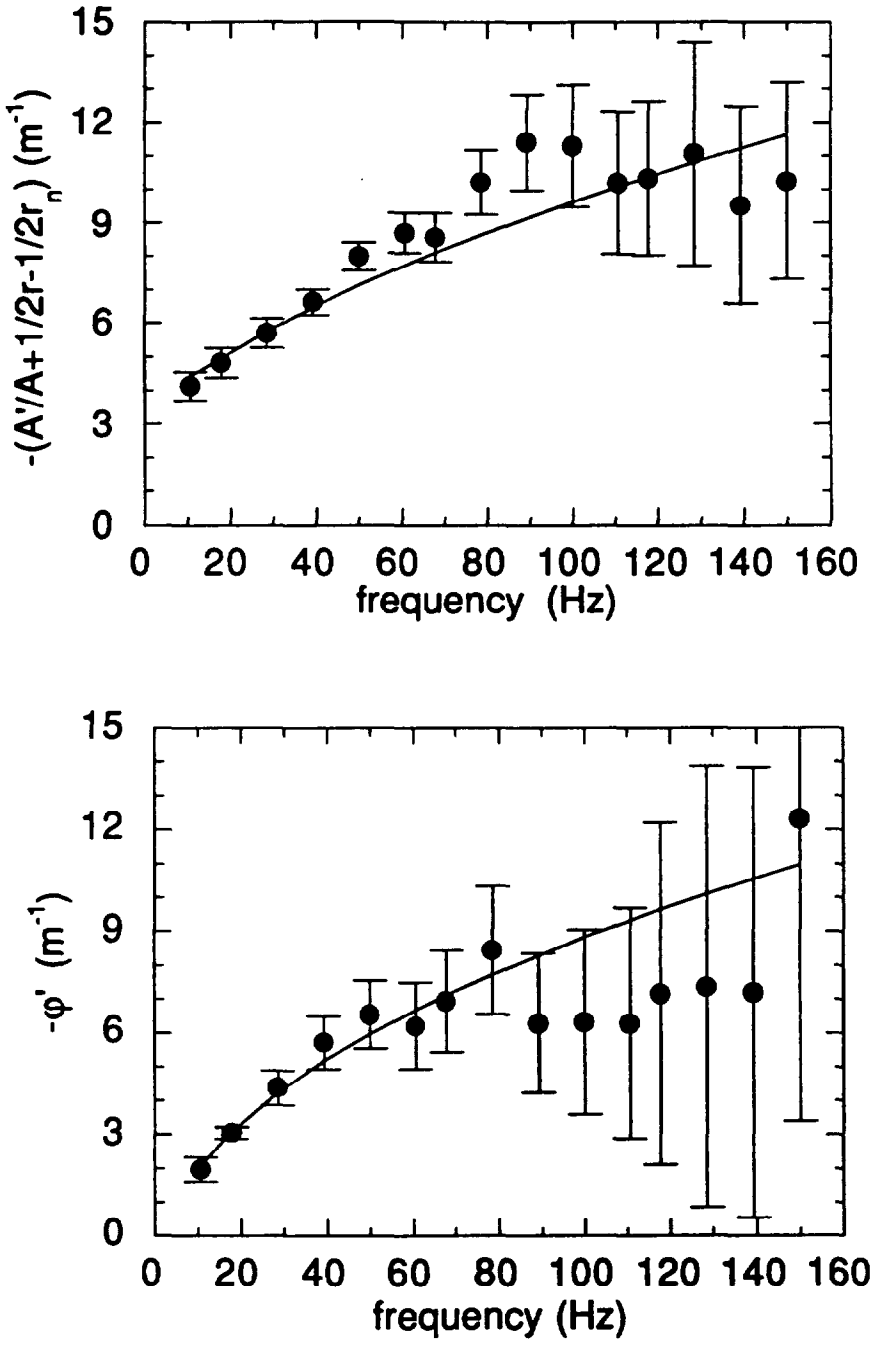

Fig.4: Statistical uncertainties on (a) $-(A'/A+1/2r+1/2r_n)(\omega)$ and (b) $-\varphi'(\omega)$ obtained as in Fig.3b. The same artificial damping, θ=25 ms, is used. The lines correspond to the unperturbed results, the points to the same perturbed case of Fig.3b. The values of $-(A'/A+1/2r+1/2r_n)$ and $-\varphi'$ have been corrected for the effect of the artificial damping.

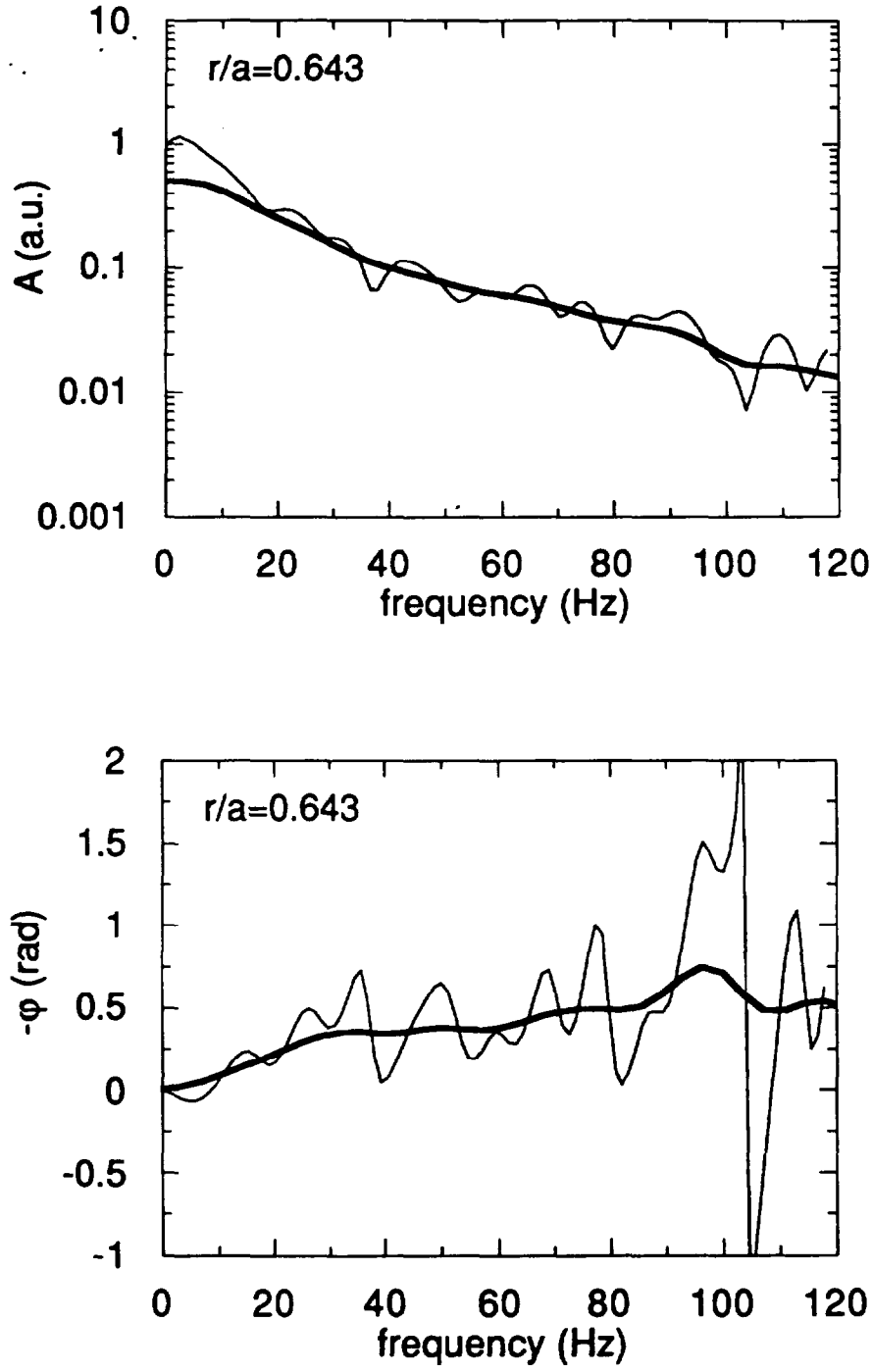

Fig.5: Square root of power spectrum (a) and cross-phase spectrum relative to the innermost channel (b) for the experimental data at r/a=0.643 of Fig.2. The thin line is the result obtained without the application of the artificial damping, while the thick line is obtained by applying the artificial damping with θ=25 ms.

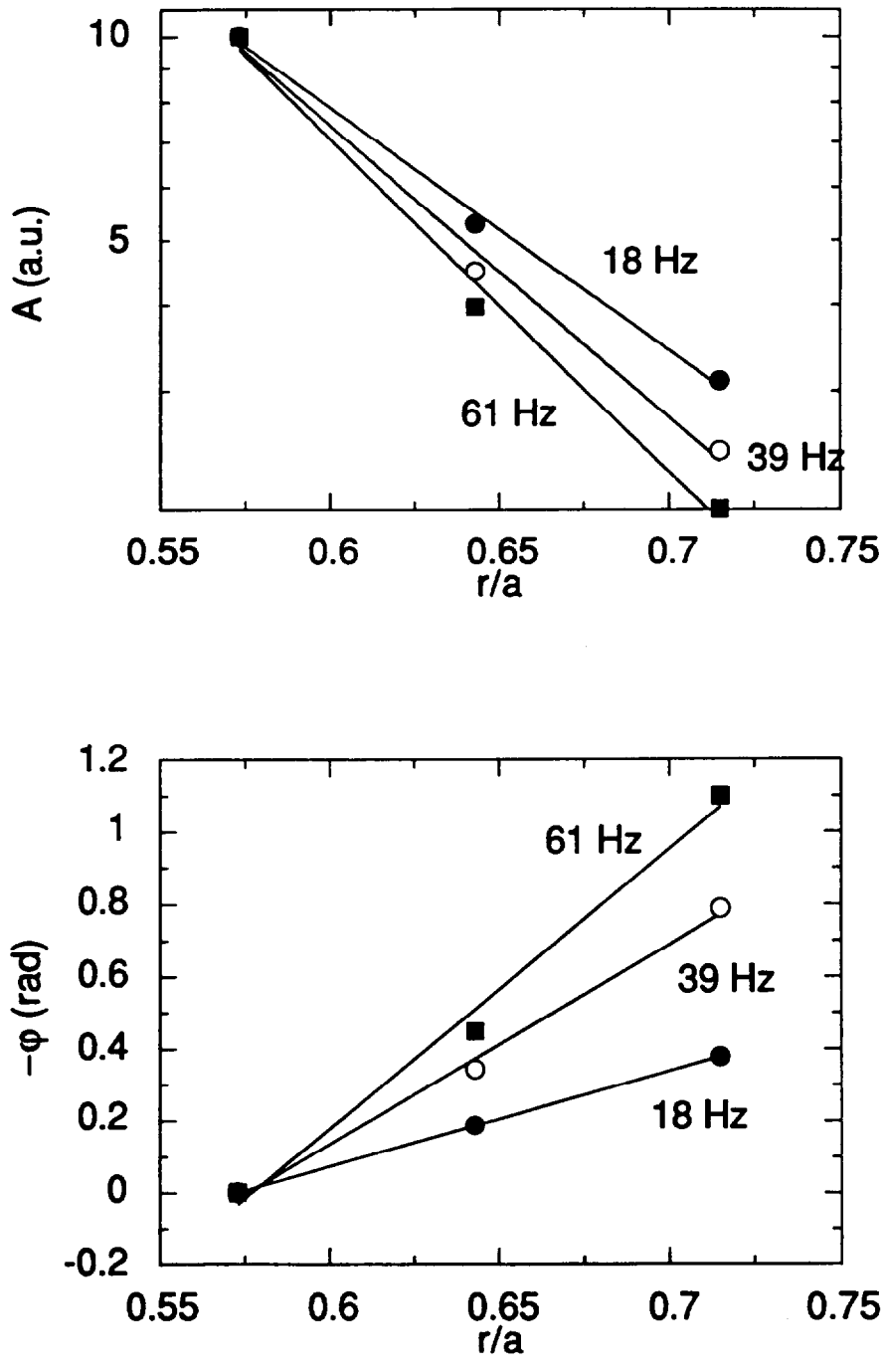

Fig.6: Amplitudes (a) and phases (b) as functions of radius at different frequencies for the experimental data of Fig.2. An artificial damping with θ=25 ms has been applied. The values of φ' and A'/A obtained by linear best-fits to the data must be corrected for the effect of the artificial damping.

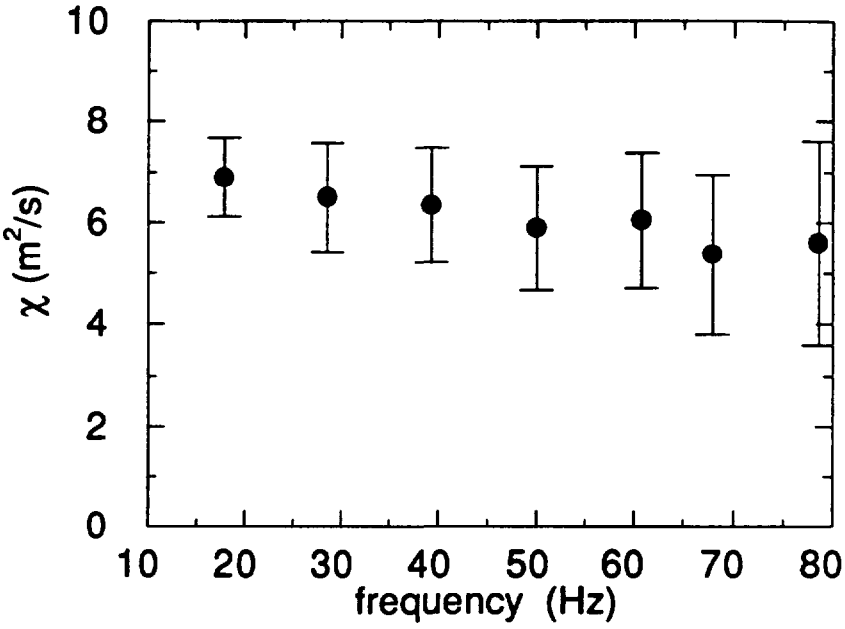

Fig.7: χ_g values determined from the linear data fits of Fig.6, plotted vs frequency. The error bars shown correspond to the statistical uncertainties derived in Fig.3b. The frequency interval of 10 Hz corresponds roughly to the bandwidth associated with the artificial damping used (θ=25 ms).

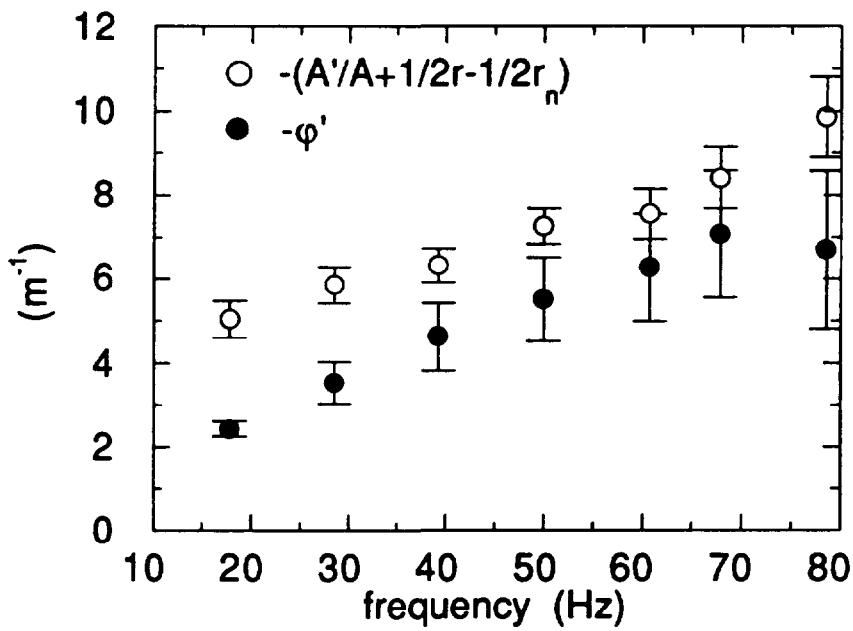

Fig.8: -($A'/A+1/2r+1/2r_n$) and -φ ' determined from the linear data fits of Fig.6, plotted vs frequency. These data have been corrected for the effect of the artificial damping. The error bars shown correspond to the statistical uncertainties derived in Fig.4.

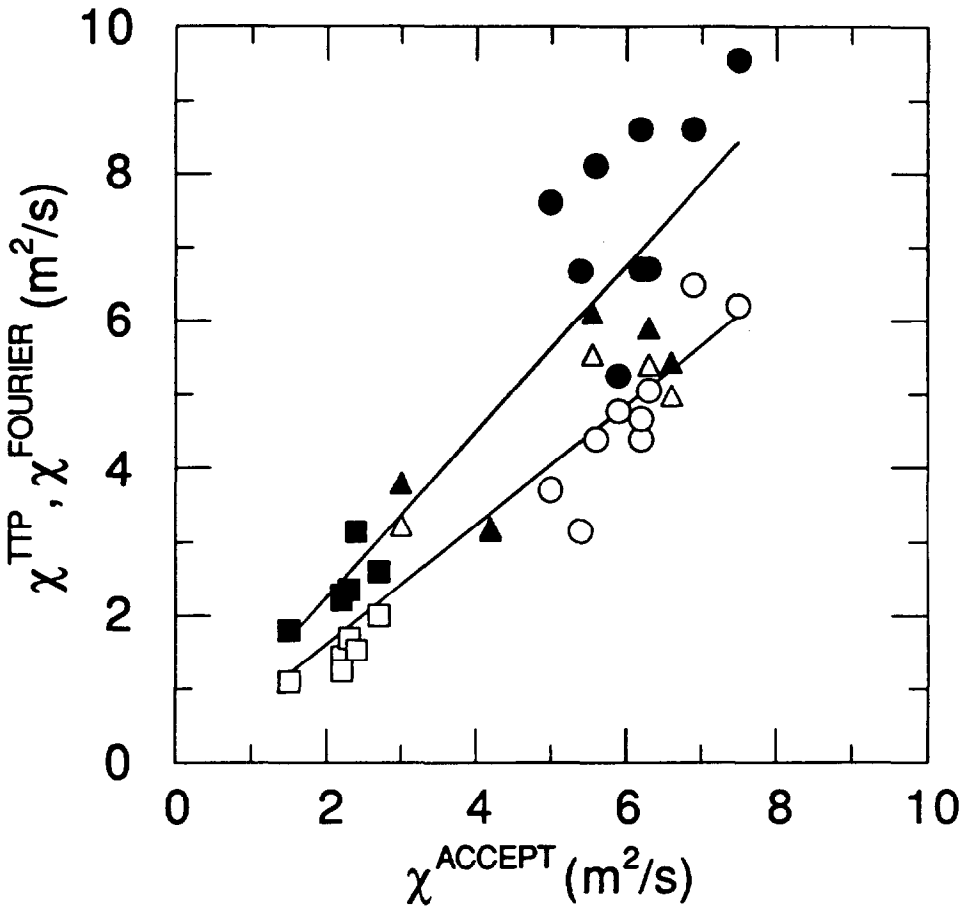

Fig.9: Comparison of the χ values obtained with different methods for 20 JET discharges. The data shown are the χ^{TTP} (open symbols) and $\chi^{FOURIER}$ (closed symbols) values plotted against χ^{ACCEPT}. Circles correspond to I_p=5 MA, triangles to I_p=3 MA, squares to I_p=2 MA. The lines are linear best-fits to the χ^{TTP} and$\chi^{FOURIER}$ values, showing systematic discrepancies <30%, with a statistical spread of about ±15%.

9/13/72

To P.E. Staff

Dear Peter,

This paper is about a method to analyse Heat Pulse data, developed by the Milano group
The final part of this paper uses published JET data and compares the method with two other methods as used by the FOM/JET groups
The FOM and JET authors are included for their help in the interpretation of the published JET data.
Both FOM and JET authors are happy with the authorship of this paper.
Is this conform JET regulations?

George Sips

JET-P(92)18

Fourier Analysis of Sawtooth Heat Pulse Propagation and Comparison with other methods using JET Data

F de Luca[1], G Gorini[1], G M D Hogeweij[2], A Jacchia[3], G Kramer, N J Lopes Cardozo[2], P Mantica[3], A C C Sips.

JET Joint Undertaking, Abingdon, Oxon, OX14 3EA.
[1] Dipartimento di Fisica, Universita degli Studi di Milano, Milano, Italy
[2] FOM Instituut voor Plasmafysica "Rijnhuizen", Associatie EURATOM-FOM, Nieuwegein, The Netherlands
[3] Instituto di Fisica del Plasma, Associazione EURATOM-ENEA-CNR, Milano, Italy.

Preprint of a paper to be submitted for publication in Nuclear Fusion

March 1992

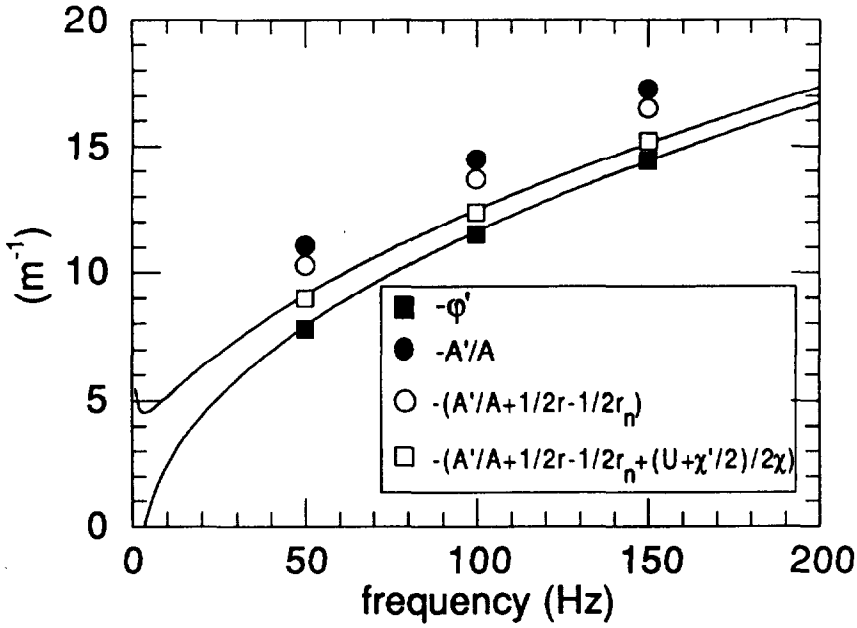

Fig.1: Numerically simulated values of $-\varphi'$ and $-A'/A$ (symbols) compared with the values predicted by Eq.3-4 (full lines). The simulated heat pulse is taken at r/a=0.5 in a cylindrical JET-like plasma (a=1.3 m) with U=10r/a m/s, χ=1+9r^2/a^2 m^2/s and τ=15 ms.

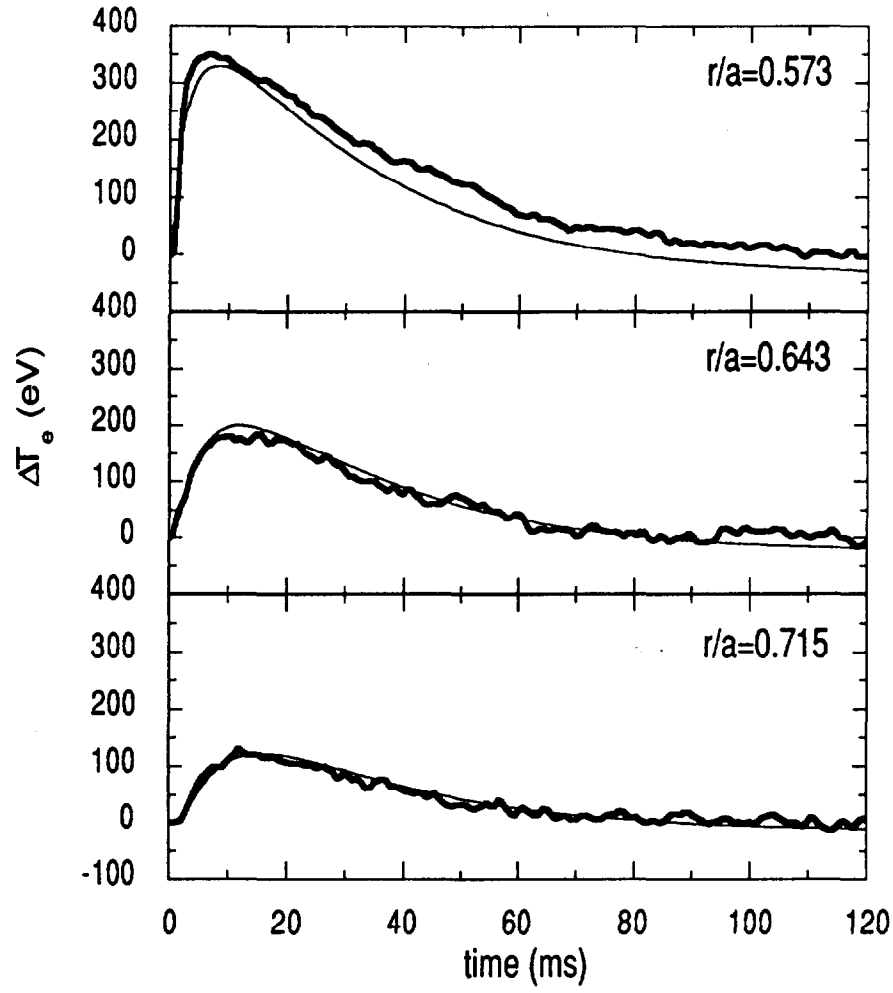

Fig.2: Average heat pulse signals obtained by coherent addition of sawtooth heat pulses for JET discharge #19619. The data (thick line) correspond to the three radial positions r/a=0.573, 0.643 and 0.715. Also shown is the best-fitted ACCEPT simulation (thin line), using a uniform χ=5.55 m^2/s and a damping time constant τ=12 ms.

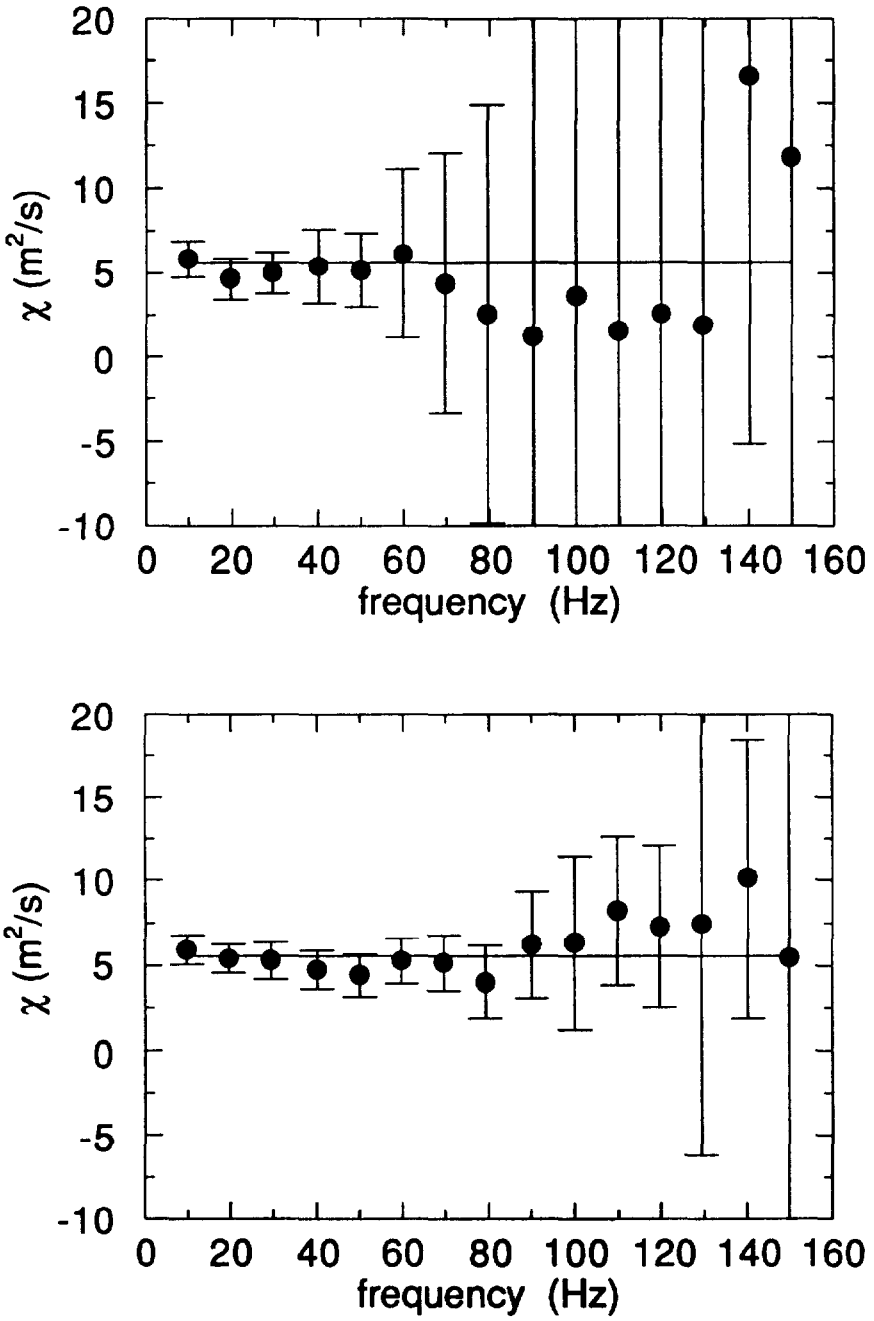

Fig.3: Statistical uncertainties on $\chi_g(\omega)$ obtained by superimposing random noise (σ=7 eV) to the ACCEPT simulation shown in Fig.2, (a) without and (b) with noise reduction using an artificial damping θ=25 ms. The line corresponds to the unperturbed result, the points to one of the many different perturbed cases considered.

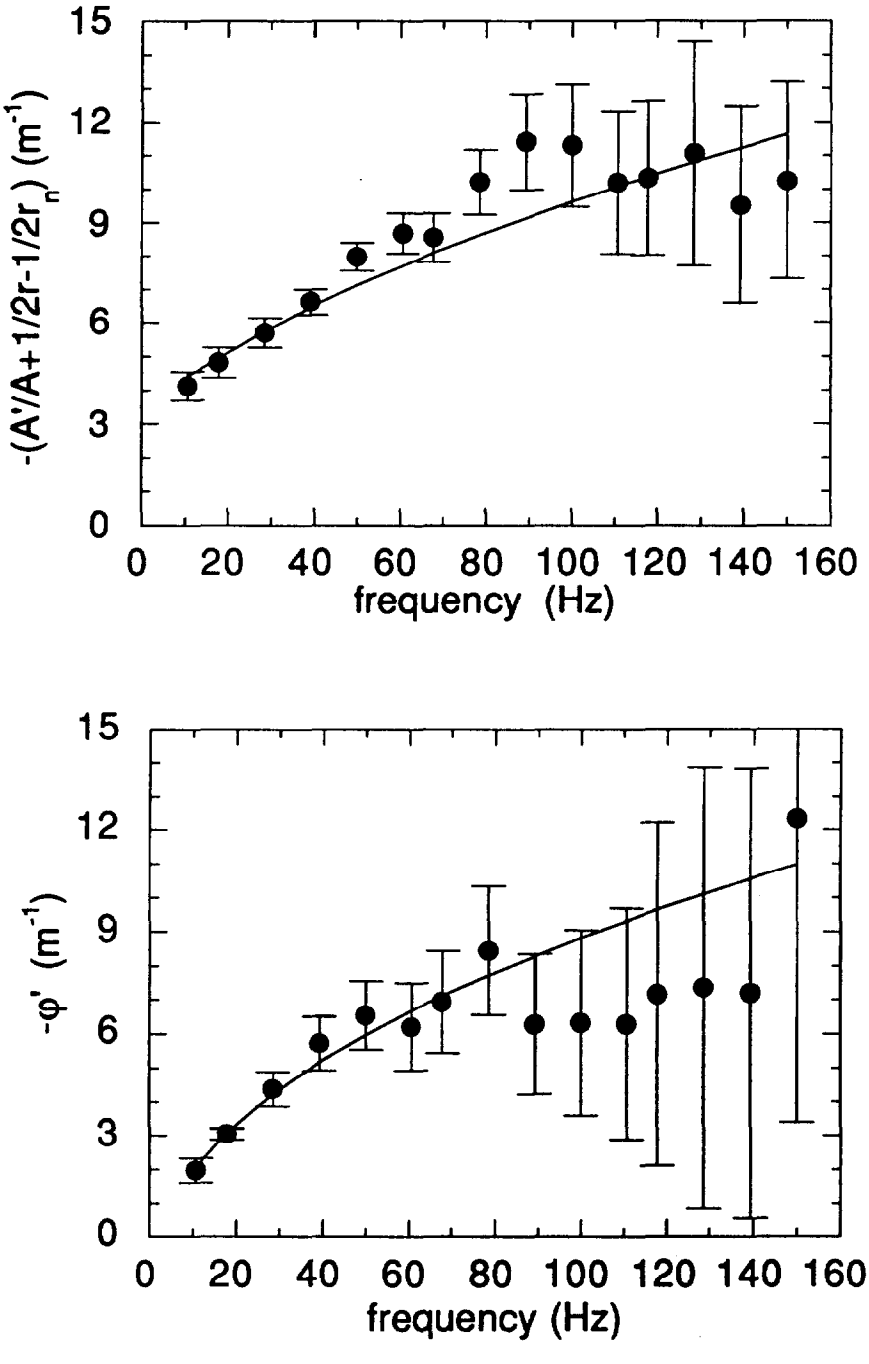

Fig.4: Statistical uncertainties on (a) $-(A'/A+1/2r+1/2r_n)(\omega)$ and (b) $-\varphi'(\omega)$ obtained as in Fig.3b. The same artificial damping, θ=25 ms, is used. The lines correspond to the unperturbed results, the points to the same perturbed case of Fig.3b. The values of $-(A'/A+1/2r+1/2r_n)$ and $-\varphi'$ have been corrected for the effect of the artificial damping.

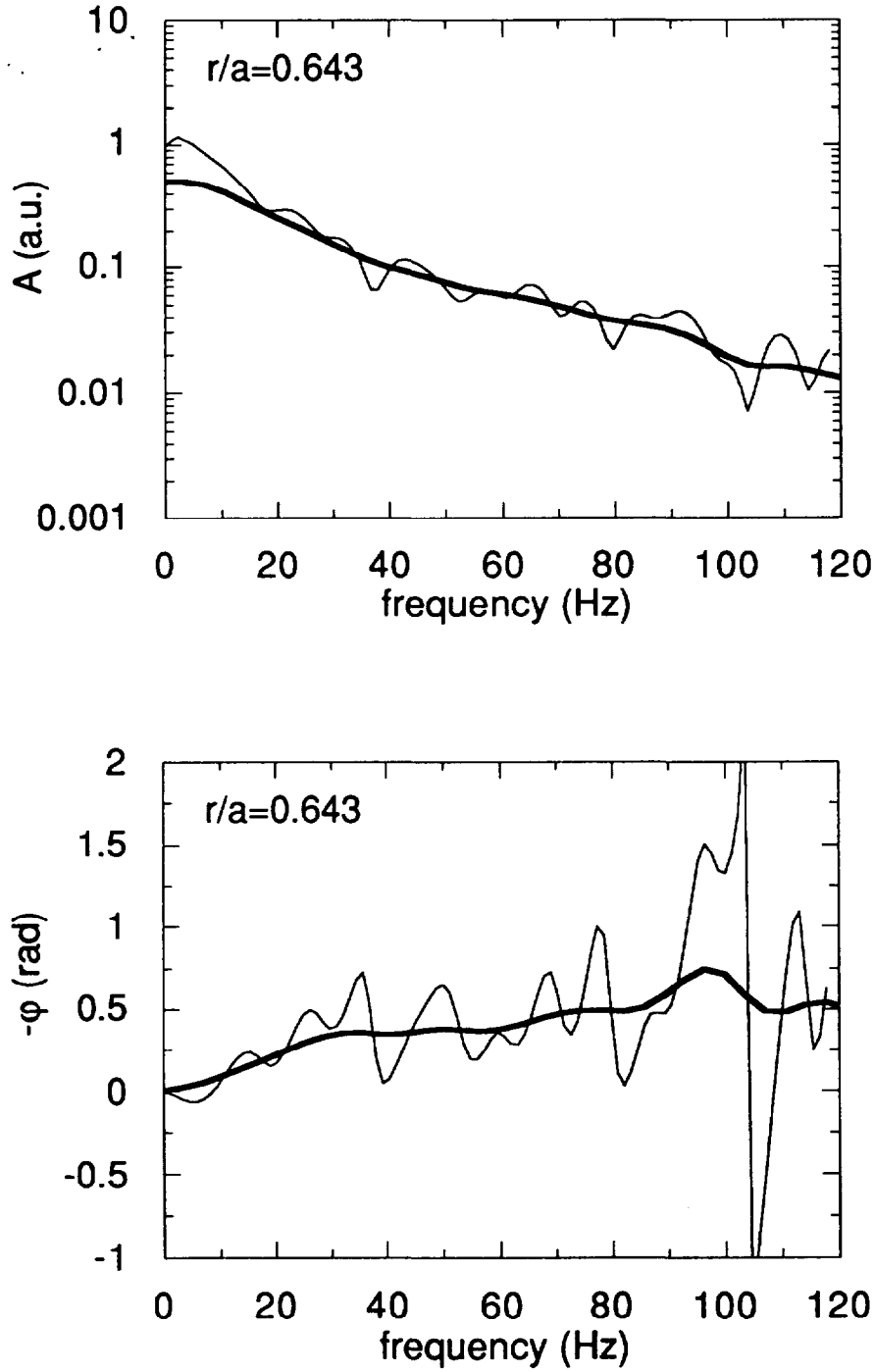

Fig.5: Square root of power spectrum (a) and cross-phase spectrum relative to the innermost channel (b) for the experimental data at r/a=0.643 of Fig.2. The thin line is the result obtained without the application of the artificial damping, while the thick line is obtained by applying the artificial damping with θ=25 ms.

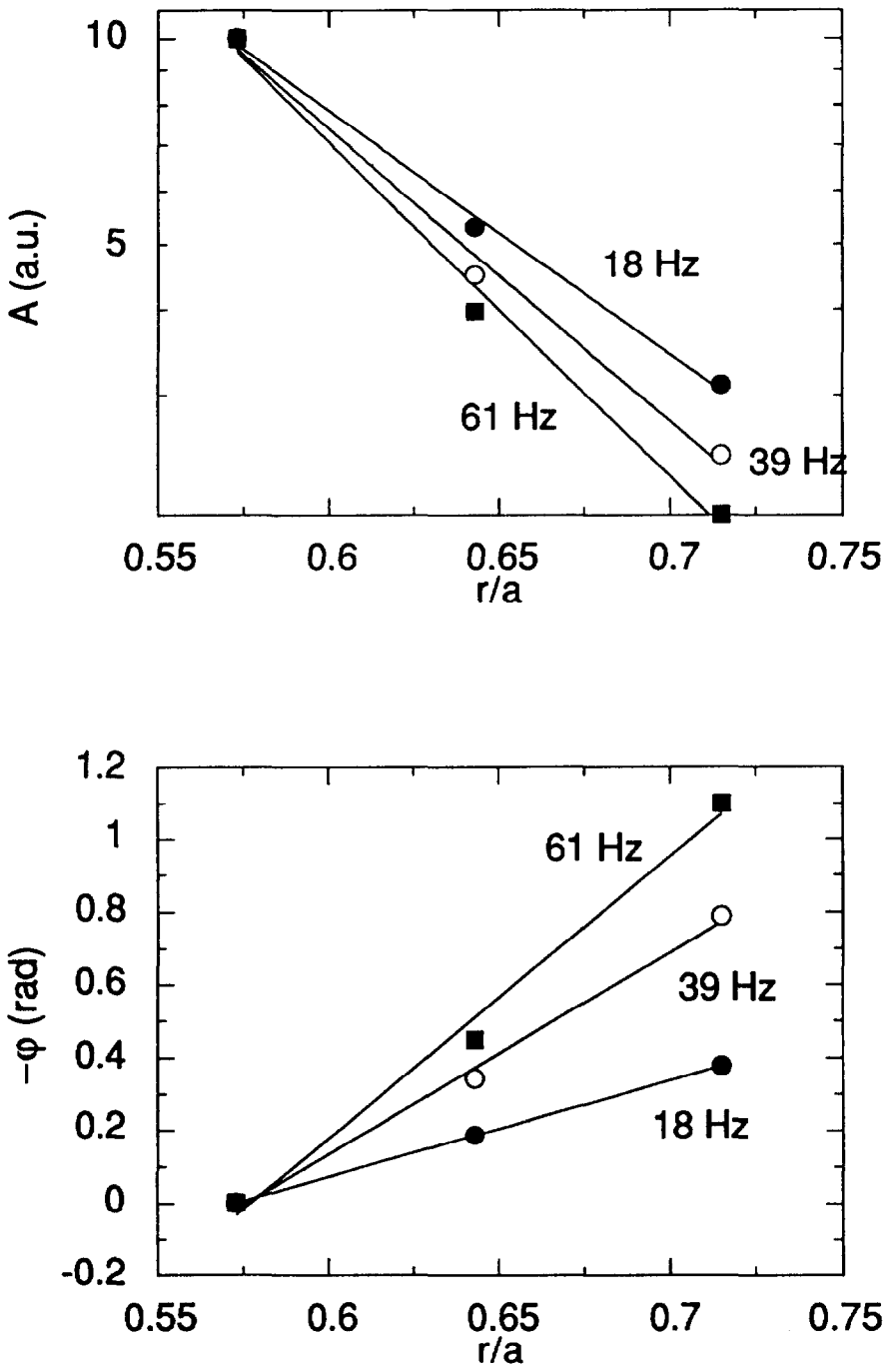

Fig.6: Amplitudes (a) and phases (b) as functions of radius at different frequencies for the experimental data of Fig.2. An artificial damping with θ=25 ms has been applied. The values of φ' and A'/A obtained by linear best-fits to the data must be corrected for the effect of the artificial damping.

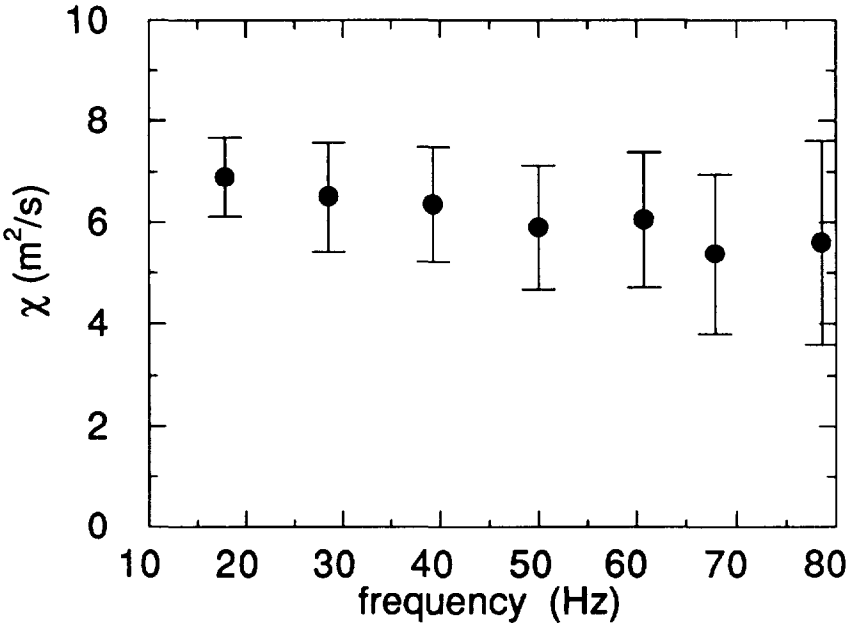

Fig.7: χ_g values determined from the linear data fits of Fig.6, plotted vs frequency. The error bars shown correspond to the statistical uncertainties derived in Fig.3b. The frequency interval of 10 Hz corresponds roughly to the bandwidth associated with the artificial damping used (θ=25 ms).

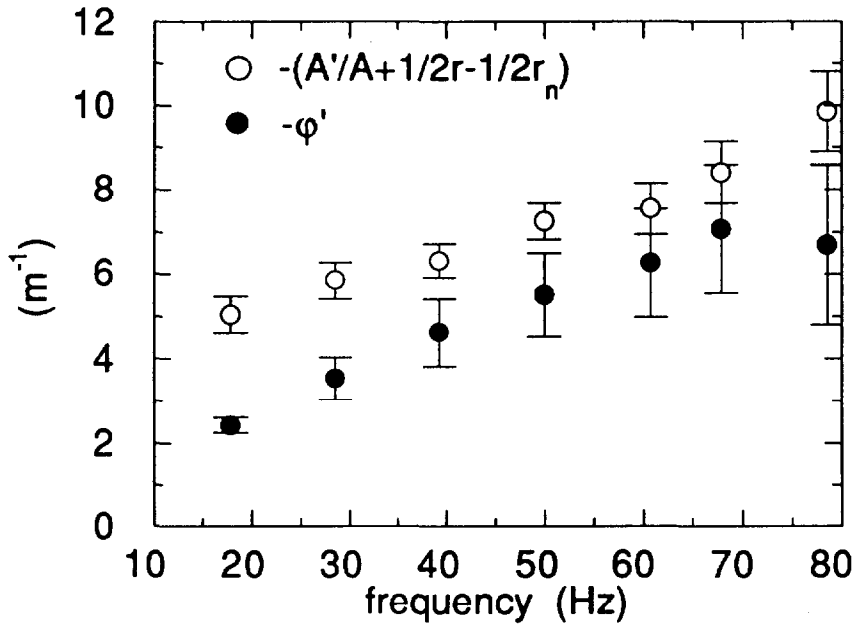

Fig.8: -(A'/A+1/2r+1/2r_n) and -φ ' determined from the linear data fits of Fig.6, plotted vs frequency. These data have been corrected for the effect of the artificial damping. The error bars shown correspond to the statistical uncertainties derived in Fig.4.

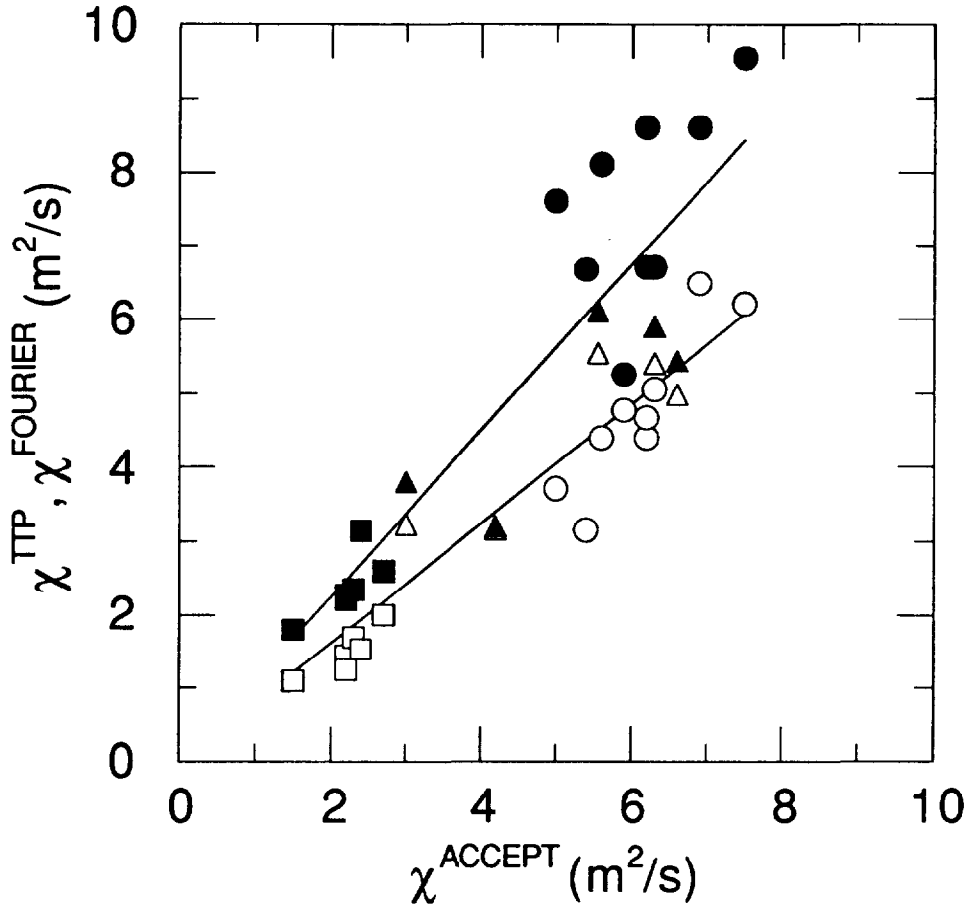

Fig.9: Comparison of the χ values obtained with different methods for 20 JET discharges. The data shown are the χ^{TTP} (open symbols) and $\chi^{FOURIER}$ (closed symbols) values plotted against χ^{ACCEPT}. Circles correspond to I_p=5 MA, triangles to I_p=3 MA, squares to I_p=2 MA. The lines are linear best-fits to the χ^{TTP} and $\chi^{FOURIER}$ values, showing systematic discrepancies <30%, with a statistical spread of about ±15%.

ANNEX

P.-H. REBUT, A. GIBSON, M. HUGUET, J.M. ADAMS[1], B. ALPER, H. ALTMANN, A. ANDERSEN[2], P. ANDREW[3], M. ANGELONE[4], S. ALI-ARSHAD, P. BAIGGER, W. BAILEY, B. BALET, P. BARABASCHI, P. BARKER, R. BARNSLEY[5], M. BARONIAN, D.V. BARTLETT, L. BAYLOR[6], A.C. BELL, G. BENALI, P. BERTOLDI, E. BERTOLINI, V. BHATNAGAR, A.J. BICKLEY, D. BINDER, H. BINDSLEV[2], T. BONICELLI, S.J. BOOTH, G. BOSIA, M. BOTMAN, D. BOUCHER, P. BOUCQUEY, P. BREGER, H. BRELEN, H. BRINKSCHULTE, D. BROOKS, A. BROWN, T. BROWN, M. BRUSATI, S. BRYAN, J. BRZOZOWSKI[7], R. BUCHSE[22], T. BUDD, M. BURES, T. BUSINARO, P. BUTCHER, H. BUTTGEREIT, C. CALDWELL-NICHOLS, D.J. CAMPBELL, P. CARD, G. CELENTANO, C.D. CHALLIS, A.V. CHANKIN[8], A. CHERUBINI, D. CHIRON, J. CHRISTIANSEN, P. CHUILON, R. CLAESEN, S. CLEMENT, E. CLIPSHAM, J.P. COAD, I.H. COFFEY[9], A. COLTON, M. COMISKEY[10], S. CONROY, M. COOKE, D. COOPER, S. COOPER, J.G. CORDEY, W. CORE, G. CORRIGAN, S. CORTI, A.E. COSTLEY, G. COTTRELL, M. COX[11], P. CRIPWELL[12], O. Da COSTA, J. DAVIES, N. DAVIES, H. de BLANK, H. de ESCH, L. de KOCK, E. DEKSNIS, F. DELVART, G.B. DENNE-HINNOV, G. DESCHAMPS, W.J. DICKSON[13], K.J. DIETZ, S.L. DMITRENKO, M. DMITRIEVA[14], J. DOBBING, A. DOGLIO, N. DOLGETTA, S.E. DORLING. P.G. DOYLE, D.F. DÜCHS, H. DUQUENOY, A. EDWARDS, J. EHRENBERG, A. EKEDAHL, T. ELEVANT[7], S.K. ERENTS[11], L.G. ERIKSSON, H. FAJEMIROKUN[12], H. FALTER, J. FREILING[15], F. FREVILLE, C. FROGER, P. FROISSARD, K. FULLARD, M. GADEBERG, A. GALETSAS, T. GALLAGHER, D. GAMBIER, M. GARRIBBA, P. GAZE, R. GIANNELLA, R.D. GILL, A GIRARD, A. GONDHALEKAR, D. GOODALL[11], C. GORMEZANO, N.A. GOTTARDI, C. GOWERS, B.J. GREEN, B. GRIEVSON, R. HAANGE, A. HAIGH, C.J. HANCOCK, P.J. HARBOUR, T. HARTRAMPF, N.C. HAWKES[11], P. HAYNES[11], J.L. HEMMERICH, T. HENDER[11], J. HOEKZEMA, D. HOLLAND, M. HONE, L. HORTON, J. HOW, M. HUART, I. HUGHES, T.P. HUGHES[10], M. HUGON, Y. HUO[16], K. IDA[17], B. INGRAM, M. IRVING, J. JACQUINOT, H. JAECKEL, J.F. JAEGER, G. JANESCHITZ, Z. JANKOVICZ[18], O.N. JARVIS, F. JENSEN, E.M. JONES, H.D. JONES, L.P.D.F. JONES, S. JONES[19], T.T.C. JONES, J.-F. JUNGER, F. JUNIQUE, A. KAYE, B.E. KEEN, M. KEILHACKER, G.J. KELLY, W. KERNER, A. KHUDOLEEV[21], R. KONIG, A. KONSTANTELLOS, M. KOVANEN[20], G. KRAMER[15], P. KUPSCHUS, R. LÄSSER, J.R. LAST, B. LAUNDY, L. LAURO-TARONI, M. LAVEYRY, K. LAWSON[11], M. LENNHOLM, J. LINGERTAT[22], R.N. LITUNOVSKI, A. LOARTE, R. LOBEL, P. LOMAS, M. LOUGHLIN, C. LOWRY, J. LUPO, A.C. MAAS[15], J. MACHUZAK[19], B. MACKLIN, G. MADDISON[11], C.F. MAGGI[23], G. MAGYAR, W. MANDL[22], V. MARCHESE, G. MARCON, F. MARCUS, J. MART, D. MARTIN, E. MARTIN, R. MARTIN-SOLIS[24], P. MASSMANN, G. MATTHEWS, H. McBRYAN, G. McCRACKEN[11], J. McKIVITT, P. MERIGUET, P. MIELE, A. MILLER, J. MILLS, S.F. MILLS, P. MILLWARD, P. MILVERTON, E. MINARDI[4], R. MOHANTI[25], P.L. MONDINO, D. MONTGOMERY[26], A. MONTVAI[27], P. MORGAN, H. MORSI, D. MUIR, G. MURPHY, R. MYRNÄS[28], F. NAVE[29], G. NEWBERT, M. NEWMAN, P. NIELSEN, P. NOLL, W. OBERT, D. O'BRIEN, J. ORCHARD, J. O'ROURKE, R. OSTROM, M. OTTAVIANI, M. PAIN, F. PAOLETTI, S. PAPASTERGIOU, W. PARSONS, D. PASINI, D. PATEL, A. PEACOCK, N. PEACOCK[11], R.J.M. PEARCE, D. PEARSON[12], J.F. PENG[16], R. PEPE DE SILVA, G. PERINIC, C. PERRY, M. PETROV[21], M.A. PICK, J. PLANCOULAINE, J.-P POFFÉ, R. PÖHLCHEN, F. PORCELLI, L. PORTE[13], R. PRENTICE, S. PUPPIN, S. PUTVINSKII[8], G. RADFORD[30], T. RAIMONDI, M.C. RAMOS DE ANDRADE, R. REICHLE, J. REID, S. RICHARDS, E. RIGHI, F. RIMINI, D. ROBINSON[11], A. ROLFE, R.T. ROSS, L. ROSSI, R. RUSS, P. RUTTER, H.C. SACK, G. SADLER, G. SAIBENE, J.L. SALANAVE, G. SANAZZARO, A. SANTAGIUSTINA, R. SARTORI, C. SBORCHIA, P. SCHILD, M. SCHMID, G. SCHMIDT[31], B. SCHUNKE, S.M. SCOTT, L. SERIO, A SIBLEY, R. SIMONINI, A.C.C. SIPS, P. SMEULDERS, R. SMITH, R. STAGG, M. STAMP, P. STANGEBY[3], R. STANKIEWICZ[32], D.F. START, C.A. STEED, D. STORK, P.E. STOTT, P. STUBBERFIELD, D. SUMMERS, H. SUMMERS[13], L. SVENSSON, J.A. TAGLE[33], M. TALBOT, A. TANGA, A. TARONI, C. TERELLA, A TERRINGTON, A TESINI, P.R. THOMAS, E. THOMPSON, K. THOMSEN, F. TIBONE, A. TISCORNIA, P. TREVALION, B. TUBBING, P. VAN BELLE, H. VAN DER BEKEN, G. VLASES, M. VON HELLERMANN, T. WADE, C. WALKER, R. WALTON[31], D. WARD, M.L. WATKINS, N. WATKINS, M.J. WATSON, S. WEBER[34], J. WESSON, T.J. WIJNANDS, J. WILKS, D. WILSON, T. WINKEL, R. WOLF, D. WONG, C. WOODWARD, Y. WU[35], M. WYKES, D. YOUNG, I.D. YOUNG, L. ZANNELLI, A. ZOLFAGHARI[19], W. ZWINGMANN

[1] Harwell Laboratory, UKAEA, Harwell, Didcot, Oxfordshire, UK.
[2] Risø National Laboratory, Roskilde, Denmark.
[3] Institute for Aerospace Studies, University of Toronto, Downsview, Ontario, Canada.
[4] ENEA Frascati Energy Research Centre, Frascati, Rome, Italy.
[5] University of Leicester, Leicester, UK.
[6] Oak Ridge National Laboratory, Oak Ridge, TN, USA.
[7] Royal Institute of Technology, Stockholm, Sweden.
[8] I.V. Kurchatov Institute of Atomic Energy, Moscow, Russian Federation.
[9] Queens University, Belfast, UK.
[10] University of Essex, Colchester, UK.
[11] Culham Laboratory, UKAEA, Abingdon, Oxfordshire, UK.
[12] Imperial College of Science, Technology and Medicine, University of London, London, UK.
[13] University of Strathclyde, Glasgow, UK.
[14] Keldysh Institute of Applied Mathematics, Moscow, Russian Federation.
[15] FOM-Institute for Plasma Physics "Rijnhuizen", Nieuwegein, Netherlands.
[16] Institute of Plasma Physics, Academia Sinica, Hefei, Anhui Province, China.
[17] National Institute for Fusion Science, Nagoya, Japan.
[18] Soltan Institute for Nuclear Studies, Otwock/Świerk, Poland.
[19] Plasma Fusion Center, Massachusetts Institute of Technology, Boston, MA, USA.
[20] Nuclear Engineering Laboratory, Lappeenranta University, Finland.
[21] A.F. Ioffe Physico-Technical Institute, St. Petersburg, Russian Federation.
[22] Max-Planck-Institut für Plasmaphysik, Garching, Germany.
[23] Department of Physics, University of Milan, Milan, Italy.
[24] Universidad Complutense de Madrid, Madrid, Spain.
[25] North Carolina State University, Raleigh, NC, USA.
[26] Dartmouth College, Hanover, NH, USA.
[27] Central Research Institute for Physics, Budapest, Hungary.
[28] University of Lund, Lund, Sweden.
[29] Laboratorio Nacional de Engenharia e Tecnologia Industrial, Sacavem, Portugal.
[30] Institute of Mathematics, University of Oxford, Oxford, UK.
[31] Princeton Plasma Physics Laboratory, Princeton University, Princeton, NJ, USA.
[32] RCC Cyfronet, Otwock/Świerk, Poland,
[33] Centro de Investigaciones Energéticas, Medioambientales y Tecnológicas, Madrid, Spain.
[34] Freie Universität, Berlin, Germany.
[35] Insitute for Mechanics, Academia Sinica, Beijing, China.